Check for updates

The perfluoroadamantoxy aluminate as an ideal weakly coordinating anion? – synthesis and first applications†

Andreas Billion, [ID] [a] Marcel Schorpp,[a] Rebecca Feser,[a] Manuel Schmitt, [ID] [a] Lea Eisele,[a] Harald Scherer,[a] Takaaki Sonoda,[b] Hajimu Kawa,[c] Burkhard Butschke [ID] [a] and Ingo Krossing [ID] *[a]

Weakly coordinating anions (WCAs) facilitate the stabilization and isolation of highly reactive and almost "naked" cations. Alkoxyaluminate-based WCAs such as $[Al(OC(CF_3)_3)_4]^-$ ($[pf]^-$) are widely used due to their synthetic accessibility and their high stability. However, small cations are still able to coordinate the oxygen atoms of the $[pf]^-$ anion or even to abstract an alkoxy ligand. The novel WCA $[Al(OC_{10}F_{15})_4]^-$ ($[pfAd]^-$; $OC_{10}F_{15}$ = perfluoro-1-adamantoxy) is characterized by a very rigid core framework, thus indicating a higher stability towards fluoride-ion abstraction (DFT calculations) and providing hope to generate less disordered crystal structures. The $[pfAd]^-$ anion was generated by the reaction of the highly acidic alcohol perfluoro-1-adamantanol $C_{10}F_{15}OH$ with $LiAlH_4$ in *o*-DFB. Li[*pfAd*] could not be synthesized free of impurities (and still contains unreacted alcohol). Yet, starting from contaminated Li[*pfAd*], the very useful pure salts Ag[*pfAd*], [Ph₃C][*pfAd*] and [H(OEt₂)₂][*pfAd*] could be synthesized. The salts were characterized by NMR spectroscopy, single-crystal X-ray diffraction and IR spectroscopy. Additionally, [NO][*pfAd*] could be synthesized containing alcohol impurities but nonetheless enabled the synthesis of the salt $P_9^+[pfAd]^-$. The synthesis of Tl[*pfAd*] in a mixture of H_2O/acetone/*o*-DFB demonstrated the water stability of the $[pfAd]^-$ anion.

Introduction

Weakly coordinating anions (WCAs)[1] enable the formation, isolation and structural characterization of reactive cations,[2] the provision of truly free coordination sites during cationic catalysis (*e.g.* silylium ion based,[3] olefin polymerization,[4] asymmetric hydrogenation[5] and hydrosilylation[6]) and inhibit the ion-pairing in ionic liquids[7] or battery electrolytes (*e.g.* Li⁺,[8] Mg²⁺ (ref. 9) or Ca²⁺ (ref. 10) ions). WCAs often have at least partially fluorinated structural units. Fluorination induces the delocalization of the negative charge over the entire entity, minimizing basic or nucleophilic sites as well as the polarizability of the anion. The size of a WCA also influences the delocalization of the negative charge, as such or in a material. Hence, the size impact of WCAs on charge transfer processes occurring in thin films was recently investigated.[11] Interestingly, increased anion size led to an increase in the relative intensity of the stimulated emissions, finally leading to a decrease of self-quenching and increased photovoltaic efficiency.[12]

Common WCA classes are halogenated alkyl- and arylborate anions (*e.g.* $[B(C_6F_5)_4]^-$ (ref. 13)), triflimidates (*e.g.* $[N(SO_2CF_3)_2]^-$ (ref. 14)), *closo*-carborate and *closo*-borate anions (*e.g.* $[HCB_{11}(CF_3)_nF_{11-n}]^-$ with n = 5, 6, 10, 11[15]) and aluminate anions $[Al(OR^F)_4]^-$ (R^F = univalent fluorinated residue). The Lewis acidic aluminum center of the latter combined with a strong aluminum–oxygen bond place fluorinated alkoxyaluminate based anions among the most widely used WCAs.[16] In addition, the $[M(OR^F)_x]^-$ (x = 4, 6) WCA-type is known for several central atoms M such as B,[7,17] Al,[7,18–20] Ta,[21] Nb[21,22] and OR^F = $OC(R)(CF_3)_2$ with R = H, CH₃, Ph and CF₃. Further, aluminates with OR^F = OC_6F_5 and OC_5F_4N are known.[23,24]

WCA-limitations

Highly electrophilic metal and non-metal cations as well as highly oxidizing cations are often part of the ionic systems

[a]Institut für Anorganische und Analytische Chemie und Freiburger Materialforschungszentrum FMF, Albert-Ludwigs-Universität Freiburg, Albertstr. 21, 79104 Freiburg, Germany. E-mail: krossing@uni-freiburg.de
[b]Institute for Materials Chemistry and Engineering, Kyushu University, 6-1 Kasuga koen, Kasuga-shi, Fukuoka, 816-8580, Japan
[c]Exfluor Research Corporation, 2350 Double Creek Drive, Round Rock, Texas 78664, USA

under investigation and in part require tailor-made anions to withstand degradation. Three properties need to be considered when deciding on a type of WCA: (i) coordination ability of the anion towards the cation (ii) electrophilic stability and (iii) oxidation stability.[1,2] Unfortunately, there is no single WCA that fulfills all requirements to stabilize the reactive cation (intermediates), which can be illustrated by example reactions of the very commonly used $[B(C_6F_5)_4]^-$ anion: it suffices to stabilize the sterically demanding silylium ion $[Si(Mes)_3]^+$ and is heavily used in silylium ion catalysis,[25] whereas being incompatible towards oxidizing agents exceeding the potential of mild $[FeCp_2]^+$ such as $[NO]^+$ or $[NO_2]^+$.[26,27] Similarly, its solvent free silver salt $Ag[B(C_6F_5)_4]$ is unknown and rather decomposes giving AgC_6F_5 and $B(C_6F_5)_3$.[28] The anions $[B(C_6F_5)_4]^-/[B(Ar^F)_4]^-$ ($Ar^F = C_6H_3$-3,5-$(CF_3)_2$) even serve as a source for the C_6F_5/Ar^F residue in the mild electrochemical synthesis of perfluorobiphenyl/^FAr-Ar^F.[29] Consequently, current research still focuses on the development of novel and more resilient 'ideal' WCAs such as the recently published WCAs $[Al(OTeF_5)_4]^-$ and $[Ga(C_2F_5)_4]^-$.[30,31]

WCAs of type $[M(OR^F)_X]^-$

The water and acid stable $[Al(OC(CF_3)_3)_4]^-$ anion (from now on $[pf]^-$) is the most utilized WCA of this class and represents a very good compromise in terms of the three mentioned properties. The preparation of $[Ag(C_2H_2)_4]^+[pf]^-$ underlines the extremely low coordination ability.[32] Further, the very high stability towards deelectronation was illustrated by a deelectronation potential of +5.0 V (with $R^F = CH(CF_3)_2$, vs. Li^+/Li).[20] The synthetic accessibility of NO^+, NO_2^+, Phenazin^F or Anthracene^{Hal} salts with fully reversible formal potentials of 0.87 to 1.42 V and in unpublished work even up to 1.89 V (vs. Fc^+/Fc) demonstrates the stability towards strongly oxidizing agents.[33,34] Achilles heel of the $[pf]^-$ anion is the still very good, but limited stability towards extraordinary strong Lewis acidic cations. Thus, solutions of the $[CCl_3]^+$ salt are stable at −20 °C and have a half-life time of 2–3 hours at RT. Large and bulky silylium ions such as $[Si(C_6Me_5)_3]^+$ are compatible with $[pf]^-$. However, small cations such as $[SiMe_3]^+$ lead to anion decomposition induced by fluoride ion abstraction.[35] Thus, in order to improve the properties of WCAs of the type $[M(OR^F)_X]^-$, an improved (preferably water stable) version is necessary. It should at least reach the properties of the $[pf]^-$ anion in terms of stability towards deelectronation and coordination, but it should surpass its properties in terms of stability against extremely Lewis acidic cations. Another issue constitutes the strong tendency of the WCA $[pf]^-$ to lead to disordered crystal structures or superstructures. Indeed, single-crystal X-ray structural analysis is of paramount importance for the characterization of many reactive-cation salts. Although we have recently published a freely downloadable tool to assist in modelling disorder in such kind of crystal structures,[36,37] intrinsically more ordered structures as induced by a suitable WCA would be helpful to facilitate structure solution/refinement and wider application.

Here we report on the synthesis and first application of Li^+, Ag^+, Ph_3C^+, Tl^+ and $H(OEt_2)_2^+$ salts of the WCA $[pfAd]^-$ (=tetrakis-perfluoro-1-adamantoxy-aluminate, $[Al(OC_{10}F_{15})_4]^-$, Fig. 1). In addition, we have reinvestigated the fluoride-ion affinities (FIA) as well as a series of related properties of various WCAs including the title compound $[pfAd]^-$.[38] D3(BJ) dispersion correction was included and a reliable approach delineated earlier by Greb et al. was further selected for the investigation.[39–41]

Results and discussion

We start with a general investigation underlining the favorable properties of the target WCA $[pfAd]^-$ based on the properties of the alcohol HOpfAd = HO-$C_{10}F_{15}$. Afterwards, the thermodynamic properties of the $[pfAd]^-$ anion are discussed along the lines of our 2004 publication[38] and underlying its potential WCA performance. Subsequently, the focus is turned to synthetic aspects and the characterization of suitable starting materials to introduce the WCA $[pfAd]^-$ into a desired ionic system.

Properties of several fluoroalcohols vs. HOpfAd

The acidity of fluorinated alcohols in solution ($pK_a(MeCN)$) and in the gas phase (gas phase acidity GA) provides a first indication towards the stability of a resulting $[Al(OR^F)_4]^-$ WCA: the higher the acidity of the alcohol, the greater is the (expected) stability of the corresponding $[Al(OR^F)_4]^-$ anion (Table 1). Here, the immense influence of perfluorination (when compared with the properties of the non-fluorinated entities) may be underlined by the experimental gas-phase acidity difference of +209 kJ mol^{-1} for HOpfAd ($C_{10}F_{15}OH$, 1321 kJ mol^{-1}) in comparison to HO-Ad ($C_{10}H_{15}OH$ 1530 kJ mol^{-1}).[42,43] In addition, all HOpfAd values collected in Table 1 exceed those of HO-$C(CF_3)_3$ and are very favorable for the projected WCA $[pfAd]^-$.

In silico study of the properties of the WCA $[pfAd]^-$ in comparison to others

We use known[38] theoretical concepts to evaluate the properties of our target WCA $[pfAd]^-$ and justify possible synthesis. Hence, the fluoride ion affinity (FIA) of the (typically hard)
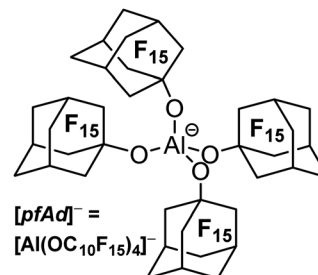

Fig. 1 Illustration of the novel WCA $[pfAd]^- = [Al(OC_{10}F_{15})_4]^-$.

Table 1 Reported experimental pK_a and log K_{AHA} values in acetonitrile; experimental and calculated (MP2/TZVPP) gas phase acidities (GA, kJ mol^{-1}) of perfluorinated alcohols including $C_{10}F_{15}OH$ as well as the non-fluorinated species

Compound	pK_a (MeCN)	log K_{AHA}	GA (exp.)	GA (calc.)
$(F_3C)_2(F_5C_6)$C-OH	22.15[44]	4.4[44]	—	1367[44]
$(F_3C)_3$C-OH	20.55[45]	4.8[45]	1355[46]	1366[44]
$C_{12}F_{15}$OH	22.00[44]	4.7[44]	—	1343[44]
HOpfAd $C_{10}F_{15}$OH	18.25[44]	4.8[44]	1321[42]	1328[44]
HO-Ad $C_{10}H_{15}$OH	—	—	1530[42]	—

Lewis acid underlying the corresponding WCA is widely used to quantify the stability of a WCA,[47] best calculated with an isodesmic $SiMe_3^+$-based reference system[48] that uses the benchmark FIA($SiMe_3^+$) of 952.5 kJ mol^{-1}.[41] Other ion affinities address further aspects: (i) the hydride ion affinity (HIA) takes soft interactions into account, (ii) the chloride (CIA) and (iii) methide ion affinities (MIA) both also consider steric contributions to Lewis acidity. Reliable ion affinity values were recently benchmarked for 183 p-block element Lewis acids by Greb *et al.*[49] Yet, the full evaluation of WCA performance needs the calculation of further properties: the HOMO-/LUMO-energy, HOMO–LUMO-Gap, partial charges q_{surf}/q_{neg}, the ligand affinity LA as well as the proton/copper decomposition reactions PD/CuD.[38] These properties were assessed for a set of ten WCAs and are discussed in detail. First, we discuss the relevant FIA values before turning to the other indicators summarized in Table 2. Note: For backward compatibility, all thermodynamic values were (re-)calculated with the computationally less demanding BP86/def-SV(P) method but including D3(BJ) dispersion correction. It was shown earlier[48] that the differences of BP86(D3BJ)/def-SV(P) calculations to benchmark DLPNO-CCSD(T)/cc-pVQZ calculations are typically small for this model chemistry and do not change the relative order. However, for forward compatibility, the thermodynamic values were additionally calculated at Greb's recommended reliable DSD-PBEP86(D3BJ)/def2-

QZVPP//pbeh3-c/def2-mSVP level of theory (second, *italic* values in Table 2).

Fluoride ion affinity of the corresponding Lewis acids. The calculated FIA value of the Lewis acid Al(OC$_{10}$F$_{15}$)$_3$, corresponding to the WCA [*pfAd*]$^-$, is with 585/*600* kJ mol^{-1} much higher than the FIA value of SbF$_5$ of 489 kJ mol^{-1} classifying it as superacidic (Table 2).[50] It is also higher than that of the Lewis acid underlying the [*pf*]$^-$ anion. Favorably, the FIA value of the Lewis acid Al(OC$_{10}$F$_{15}$)$_3$ is in the same order of magnitude as the extreme FIA values of the Lewis acids underlying the recent anions [M(OC$_5$F$_4$N)$_4$]$^-$ (with M = B, Al)[23] and [M(OTeF$_5$)$_4$]$^-$ (with M = Al, Ga).[31,51] As a final proof for the exceptional FIA value of Al(OC$_{10}$F$_{15}$)$_3$, additional DLPNO-CCSD(T)/cc-pVQZ calculations were performed as proposed by the group of Greb.[41] The calculation at this most reliable level resulted in a FIA of 596 kJ mol^{-1} for the Lewis acid Al(OC$_{10}$F$_{15}$)$_3$ and agrees within 11 kJ mol^{-1} to those collected in Table 2. With the exception of the [M(OTeF$_5$)$_4$]$^-$ WCAs, the FIAs differ by less than 15 kJ mol^{-1} to the values calculated with Greb's recommended DSD-PBEP86(D3BJ)/def2-QZVPP//pbeh3-c/def2-mSVP level of theory. Yet, due to the difference to the [M(OTeF$_5$)$_4$]$^-$ WCAs, we will continue to use and discuss only the values from Greb's approach.

The Ligand affinity (LA) defines the abstraction of a ligand from the Lewis acidic central atom of the WCA and is always endothermic. The highest value collected in Table 2 (417 kJ mol^{-1}, [Ga(C$_2$F$_5$)$_4$]$^-$) indicates good stability towards ligand abstraction. However, the LA also includes the intrinsic stability of the freed ligand. Consequently, released stable perfluorinated alcoholates result in lower LA values and thus the stability of the corresponding anion tends to be underestimated. Nevertheless, the [*pfAd*]$^-$ anion has with 388 kJ mol^{-1} the second highest entry in Table 2, further supporting its excellent stability.

The stability of the WCAs towards hard and soft electrophiles can be calculated isodesmically considering decomposition reactions with hard H$^+$ for **proton decomposition PD** and soft Cu$^+$ for **copper decomposition CuD**. Herein, the contribution of the intrinsic stability of the freed fragment is

Table 2 Comparison of calculated thermodynamic properties of widely used and recently published Lewis acids and the corresponding anions (BP86/def-SV(P) level with D3(BJ) dispersion)/(DSD-PBEP86(D3BJ)/def2-QZVPP//pbeh3-c/def2-mSVP level of theory as described by Greb *et al.*[49])

Anion	Sym.	FIA/kJ mol^{-1}	LA/kJ mol^{-1}	PD/kJ mol^{-1}	CuD/kJ mol^{-1}	HOMO/eV	Gap/eV	q_{neg}	q_{surf}
[B(OCH(CF$_3$)$_2$)$_4$]$^-$	S_4	404/*391*	301/*284*	−1140/*−1164*	−483/*−446*	−3.37	7.11	−0.21 F	−0.21 F
[B(C$_6$F$_5$)$_4$]$^-$	S_4	449/*441*	329/*341*	−1177/*−1164*	−494/*−442*	−3.11	4.22	−0.95 B	−0.22 F
[Ga(C$_2$F$_5$)$_4$]$^-$	C_1	479/*501*	401/*417*	−1174/*−1154*	−466/*−389*	−3.07	6.28	−0.22 Ga	−0.20 F
[B(OC$_5$F$_4$N)$_4$]$^-$	C_1	494/*465*	263/*246*	−1067/*−1094*	−425/*−400*	−3.64	4.17	−0.21 N	−0.21 N
[Al(OC(CF$_3$)$_3$)$_4$]$^-$	S_4	535/*547*	352/*366*	−1024/*−1020*	−377/*−317*	−4.11	6.86	−0.24 O	−0.20 F
[Al(C$_6$F$_5$)$_4$]$^-$	S_4	539/*546*	367/*373*	−1139/*−1132*	−456/*−410*	−3.35	4.29	−0.21 F	−0.21 F
[Al(OTeF$_5$)$_4$]$^-$	S_4	545/*603*	293/*339*	−981/*−950*	−394/*−282*	−6.17	2.93	−0.47 O	−0.40 F
[Ga(OTeF$_5$)$_4$]$^-$	S_4	545/*571*	308/*325*	−966/*−964*	−379/*−296*	−6.09	2.79	−0.46 O	−0.40 F
[Al(OC$_5$F$_4$N)$_4$]$^-$	C_1	581/*588*	352/*363*	−979/*−977*	−337/*−283*	−3.80	4.37	−0.22 N	−0.21 F
[Al(OC$_{10}$F$_{15}$)$_4$]$^-$	C_1	585^a/*600*	379/*388*	−959/*−963*	−325/*−271*	−4.53	4.75	−0.29 O	−0.24 F

^{a} 596 kJ mol^{-1} at the very reliable DLPNO-CCSD(T)/cc-pVQZ level. Abbreviations: fluoride ion affinity (FIA), ligand affinity (LA), proton induced decomposition (PD), copper induced decomposition (CuD), highest occupied molecular orbital (HOMO), Gap between HOMO and LUMO (lowest unoccupied molecular orbital), partial charges on the surface (q_{surf}) and most negative partial charges (q_{neg}).
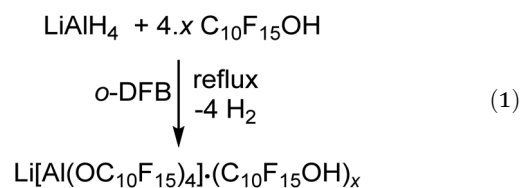
eliminated. PD and CuD are always exothermic due to the reaction of a gaseous anion and a gaseous cation under formation of two neutral molecules. The less negative the values obtained are, the more stable the corresponding WCA is towards an attack by electrophiles. Once again, promising values were obtained for the $[pfAd]^-$ anion, which improve on the frequently used $[pf]^-$ anion. The PD values amount to −963 kJ mol^{-1} compared to −1020 kJ mol^{-1} and the CuD values amount to −271 kJ mol^{-1} compared to −317 kJ mol^{-1} in favor of the $[pfAd]^-$ anion. Also, the **HOMO** energy is with −4.53 eV by 0.42 eV more favorable/lower than the HOMO of the $[pf]^-$ anion and thus less susceptible to oxidation. This oxidation stability goes along with an increased reduction sensitivity, as the **HOMO–LUMO gap** of the $[pfAd]^-$ anion is 2.11 eV lower compared to the $[pf]^-$ anion (see below). An indication of the coordination ability of an anion is provided by q_{neg} and q_{surf}. In general, the most negatively charged atom (q_{neg}) shows the greatest tendency towards coordination. However, the steric crowding around the most basic sites need to be considered. Therefore, the most negatively charged but accessible atom (q_{surf}) is of greater interest. The oxygen atoms carry the largest negative charges in the $[pfAd]^-$ anion but are not accessible due to the sterically demanding adamantoxy cages. The $[pfAd]^-$ anion tends to be slightly more coordinating compared to the $[pf]^-$ anion, but not as strongly coordinating as the $OTeF_5$-based anions with much higher O- and F-charges in Table 2.

Fluoride ion abstraction from $[pfAd]^-$ compared to $[pf]^-$. While the FIA and the LA allow a statement regarding the thermodynamic stability of an anion towards removal of a univalent ligand, the susceptibility of the fluorinated ligands in the $[pf]^-$ and the novel $[pfAd]^-$ anion themselves towards fluoride abstraction were calculated additionally (BP86(D3BJ)/def-SV(P) level). For the $[pf]^-$ anion, this is a known mode of degradation yielding, probably *via* an adduct, the epoxide C_4F_8O and the Lewis acid $Al(OC(CF_3)_3)_3$ as shown in Scheme 1 (3). This degradation reaction proceeds for example by reaction of Me_3SiCl with $Ag[pf]$, generating the strong electrophile Me_3Si^+ *in situ*.[35] The calculated reaction enthalpy for this decomposition process amounts to +600 kJ mol^{-1} when calculated in an isodesmic procedure using the experimental FIA value of COF_2 of +209 kJ mol^{-1} as anchor point, as shown in Scheme 1(3). For the $[pfAd]^-$ anion, a distinction between the abstraction of a fluoride ion of a CF group compared to the abstraction of a CF_2 group leading to several conceivable decomposition products is necessary. A comparable epoxide for the $[pfAd]^-$ anion, which results from the fluoride ion abstraction of a CF_2 group is significantly less favored with +805 kJ mol^{-1}, Scheme 1(2). Instead, fluoride ion abstraction of a CF_2 group provides a structure that hardly deviates geometrically from the anion. This decomposition pathway tends to be more favored with $\Delta_R H° = +690$ kJ mol^{-1}, Scheme 1(2). The most likely fluoride ion abstraction process is that of a CF group ($\Delta_R H° = +590$ kJ mol^{-1}), which is found in the same order of magnitude as for the $[pf]^-$ anion, Scheme 1(1). Additionally, the solvent influence on the decomposition pro-

cesses was considered and the Gibbs free enthalpies were calculated with the COSMO solvation model in CH_2Cl_2 (ε = 8.93[52]) and *o*-DFB (ε = 13.38[52]). All investigated decay processes are about 150 kJ mol^{-1} more favorable in solution than in the gas phase and tend to be more favored in *o*-DFB over CH_2Cl_2 by about 10 kJ mol^{-1}. The fluoride ion abstraction from a CF group (1) still represents the preferred decay process. Furthermore, steric shielding of the oxygen atoms as well as the inner fluorine atoms result in an increased kinetic stability, which in turn would favor decay mechanism (1) under opening of the adamantane cage. Overall, the majority of calculations show improved thermodynamic properties for the $[pfAd]^-$ anion compared to the $[pf]^-$ anion that justify the synthesis and investigation of $[pfAd]^-$ salts.

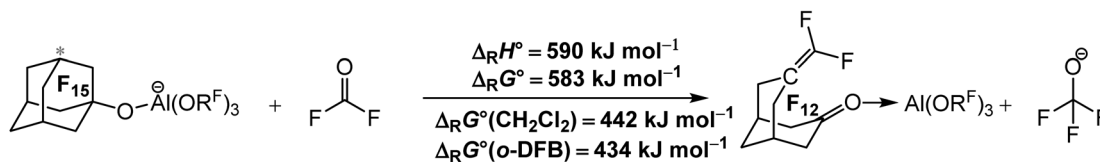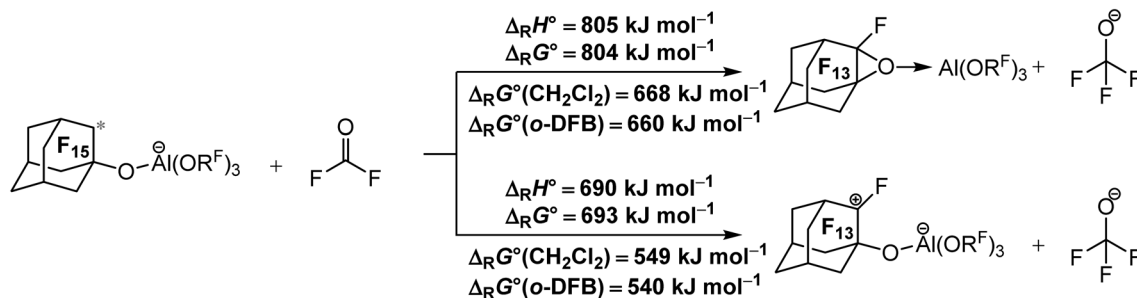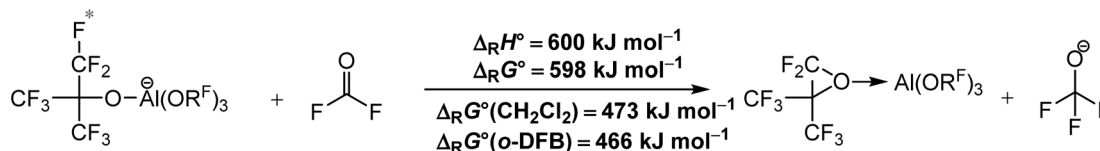### Towards the pure Li[*pfAd*] salt: unexpected synthetic challenges

The synthesis of Li[*pfAd*] (**1**) turned out to be non-trivial. Hence, straightforward reaction of $LiAlH_4$ and $C_{10}F_{15}OH$ in hexane, heptane, toluene, ether, THF *etc.* according to the established synthesis protocol for $Li[Al(OC(CF_3)_3)_4]$[18] does **not** work as expected. In order to prevent side reactions caused by strongly hydrogen-bonded water, the alcohol had to be dried in *o*-DFB solution over activated 3 Å molecular sieves prior to use. Since $C_{10}F_{15}OH$ is one of the most acidic alcohols known, a non-negligible content of $NaOC_{10}F_{15}$ forms from reaction with the sieves. Hence, the dried alcohol must be sublimed at least twice afterwards to remove any alkoxide traces. Reaction between $LiAlH_4$ and this dried purified alcohol $C_{10}F_{15}OH$ in the weakly coordinating solvent toluene does not proceed even at reflux and under ultrasonic activation. However, reaction of 4.6 equiv. of $C_{10}F_{15}OH$ with $LiAlH_4$ in *o*-DFB results in an immediate evolution of gas (eqn (1)).

$$LiAlH_4 \ + 4.x \ C_{10}F_{15}OH$$

$$o\text{-DFB} \ \Big\downarrow \begin{array}{l} \text{reflux} \\ \text{-4 } H_2 \end{array} \qquad (1)$$

$$Li[Al(OC_{10}F_{15})_4]\cdot(C_{10}F_{15}OH)_x$$

After the gas evolution was finished, indicating the complete turnover, and cooling down the reaction mixture, precipitation of a small amount of a colorless solid was observed. Multinuclear NMR spectroscopy of the precipitated solid and the reaction solution showed resonances caused by the target compound Li[*pfAd*] (**1**) as well as unreacted alcohol $C_{10}F_{15}OH$. Adding a small amount of $C_{10}F_{15}OH$ to an already measured NMR sample leads to a distinct increase in the intensity of the alcohol resonances confirming the impurity as the alcohol. Furthermore, integration of the resonances of the alcohol and the solvent *o*-DFB in the ^{1}H- and ^{19}F NMR spectra yielded the same stoichiometric ratio providing evidence for the absence of alkoxide $C_{10}F_{15}O^-$ (for details see ESI†).

Purification attempts of Li[*pfAd*]. After the solvent *o*-DFB was removed, the obtained solid was attempted to be purified by extraction with *o*-DFB, washing with toluene, C_6F_6, CH_2Cl_2

(1) Fluoride abstraction from a CF group of the [*pfAd*]⁻ anion

$$\Delta_R H° = 590 \text{ kJ mol}^{-1}$$
$$\Delta_R G° = 583 \text{ kJ mol}^{-1}$$
$$\Delta_R G°(CH_2Cl_2) = 442 \text{ kJ mol}^{-1}$$
$$\Delta_R G°(o\text{-DFB}) = 434 \text{ kJ mol}^{-1}$$

(2) Fluoride abstraction from a CF₂ group of the [*pfAd*]⁻ anion

$$\Delta_R H° = 805 \text{ kJ mol}^{-1}$$
$$\Delta_R G° = 804 \text{ kJ mol}^{-1}$$
$$\Delta_R G°(CH_2Cl_2) = 668 \text{ kJ mol}^{-1}$$
$$\Delta_R G°(o\text{-DFB}) = 660 \text{ kJ mol}^{-1}$$

$$\Delta_R H° = 690 \text{ kJ mol}^{-1}$$
$$\Delta_R G° = 693 \text{ kJ mol}^{-1}$$
$$\Delta_R G°(CH_2Cl_2) = 549 \text{ kJ mol}^{-1}$$
$$\Delta_R G°(o\text{-DFB}) = 540 \text{ kJ mol}^{-1}$$

(3) Fluoride abstraction from a CF₃ group of the [*pf*]⁻ anion

$$\Delta_R H° = 600 \text{ kJ mol}^{-1}$$
$$\Delta_R G° = 598 \text{ kJ mol}^{-1}$$
$$\Delta_R G°(CH_2Cl_2) = 473 \text{ kJ mol}^{-1}$$
$$\Delta_R G°(o\text{-DFB}) = 466 \text{ kJ mol}^{-1}$$

Scheme 1 Calculated isodesmic reaction enthalpies $\Delta_R H°$ and Gibbs free energies $\Delta_R G°$ for the decomposition of the [Al(OR^F)$_4$]⁻ WCAs ((1) and (2) R^F = C$_{10}$F$_{15}$), (3) (R^F = C(CF$_3$)$_3$) under fluoride ion abstraction (BP86/def-SV(P) level with D3(BJ) dispersion). Solvation effects on the Gibbs free energy $\Delta_R G°$ were considered by using the COSMO solvation model for CH$_2$Cl$_2$ ($\varepsilon = 8.93^{52}$) and o-DFB ($\varepsilon = 13.38^{52}$). The red star marks the abstracted fluoride ion. The experimental FIA of COF$_2$ of 209 kJ mol⁻¹ was used as an anchor point for comparison.

and water without success. In addition, the Li-salt could not be crystallized. In contrast to Li[*pf*],[18] Li[*pfAd*] (**1**) cannot be purified by sublimation at 180 °C in dynamic vacuo. However, the experiments showed that the anion is stable for several hours at elevated temperatures as well as demonstrating its stability towards air and moisture. To avoid larger amounts of unreacted alcohol, the reaction was carried out with 4.1 eq. of C$_{10}$F$_{15}$OH, which again led to the formation of **1** but the NMR spectra still showed further unreacted alcohol (approx. 29 mol%) even after a prolonged reaction time of 3 d. Subsequently, stoichiometric ratios containing less than 4.0 eq. of C$_{10}$F$_{15}$OH were investigated targeting a mixture of Li[H$_x$Al(OC$_{10}$F$_{15}$)$_{4-x}$] (x = 0–4). With certainty, the NMR-spectra recorded in THF counter-intuitively show the presence of unreacted alcohol although a high reactivity between LiAlH$_4$ and C$_{10}$F$_{15}$OH would be expected. Potentially these observations indicate that the alcohol C$_{10}$F$_{15}$OH is coordinated to the hard ion Li⁺ and therefore cannot be removed entirely. The substitution of the Li⁺ ion with the slightly softer and larger Na⁺ ion was expected to resolve the strong alcohol coordination. For this purpose, NaAlH$_4$ was reacted with C$_{10}$F$_{15}$OH in o-DFB. The synthesis of the target compound free of impurities could again not be achieved. In addition to the previously discussed impurities in the case of the lithium salt, very small

amounts of [F–Al(OC$_{10}$F$_{15}$)$_3$]⁻ could also be verified by NMR spectroscopy (for details see ESI†).

Optimized protocol. To sum up our experience, the best synthesis of **1**, albeit not being free of alcohol impurity, consists of the reaction of excess alcohol (here 4.5 eq.) with LiAlH$_4$ at reflux with a reaction time of 3 h followed by removal of the solvent under reduced pressure, washing with toluene for three times and drying of the obtained colorless solid under reduced pressure at elevated temperatures (here 100 °C). Based on this synthesis protocol, the reaction was carried out in up to 5 g scale obtaining Li[*pfAd*]·(C$_{10}$F$_{15}$OH)$_x$ with x = 0.43 and 96% yield.

Purifying Li[*pfAd*]·(C$_{10}$F$_{15}$OH)$_x$ by derivatization to target salts Cat⁺[*pfAd*]⁻

Since we could only obtain Li[*pfAd*]·(C$_{10}$F$_{15}$OH)$_x$ with excess alcohol, we targeted converting the (impure) lithium salt into useful starting materials that are pure products and free of alcohol.

Ag[*pfAd*] (2). Silver(ı) salts of WCAs are highly potent reagents for the abstraction of halogens and further can function as oxidants in which the silver ion is reduced to the metal.[53] The synthesis of **2** proceeds according to eqn (2) by

reaction of Li[*pfAd*]·(C$_{10}$F$_{15}$OH)$_x$ with AgF in *o*-DFB under ultrasonic activation.
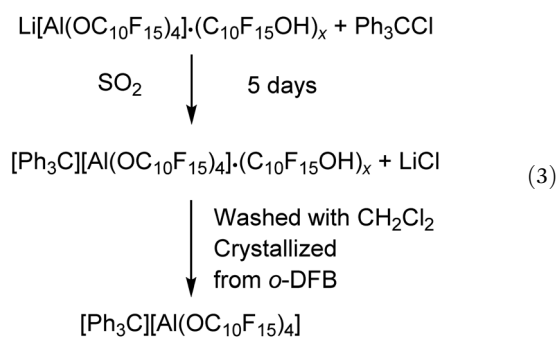
$$\text{Li[Al(OC}_{10}\text{F}_{15}\text{)}_4]\cdot(\text{C}_{10}\text{F}_{15}\text{OH})_x + \text{AgF}$$

$$o\text{-DFB} \downarrow \text{ ultrasonic activation}$$

$$\text{Ag[Al(OC}_{10}\text{F}_{15}\text{)}_4]\cdot(\text{C}_{10}\text{F}_{15}\text{OH})_x + \text{LiF} \qquad (2)$$

$$\text{Crystallized} \downarrow \text{ from CH}_2\text{Cl}_2$$

$$\text{Ag(CH}_2\text{Cl}_2\text{)}_2[\text{Al(OC}_{10}\text{F}_{15}\text{)}_4]$$
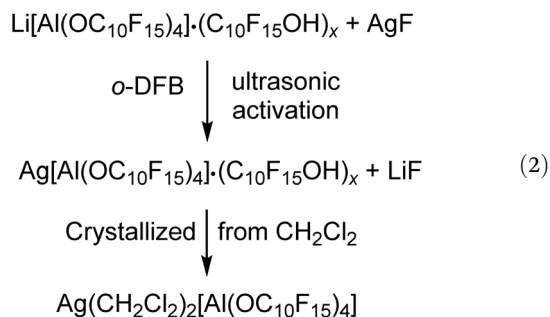
The analysis of the reaction solution of the first attempt showed resonances in the ^{19}F NMR spectrum indicating impurities by the alkoxide C$_{10}$F$_{15}$O$^-$, since the proton resonance of the alcohol was missing. This agrees with the fact that the alcohol was not sublimed prior to the synthesis of the Li[*pfAd*] (**1**) resulting in a contamination by NaOC$_{10}$F$_{15}$ (from the molecular sieves) and AgOC$_{10}$F$_{15}$, respectively, after derivatization with AgF. Subsequent gas phase diffusion crystallization with *n*-pentane resulted in the growth of two different kinds of crystals. The structures were determined as [Ag(*o*-DFB)$_2$][*pfAd*] (**2-*o*DFB**) and [Ag$_3$(OC$_{10}$F$_{15}$)$_2$(*o*-DFB)$_3$][*pfAd*] (**3**) confirming the presence of alkoxide as well as demonstrating the crucial need to sublime the alcohol prior to use. Yet, with these precautions, the silver salt was obtained free of impurities after extraction with CH$_2$Cl$_2$ and crystallization by gas phase diffusion with *n*-pentane (yield: 40%, each Ag$^+$ coordinated with two CH$_2$Cl$_2$ molecules). Multinuclear NMR spectroscopy of **2** in CD$_2$Cl$_2$ shows three resonances in the ^{19}F NMR spectrum located at $\delta_F = -121.6$ and -122.0 ppm for the 48 CF$_2$ fluorine atoms and at $\delta_F = -223.4$ ppm for the 12 CF fluorine atoms. A major resonance in the ^{27}Al NMR spectrum at $\delta_{Al} = 34.7$ ppm, consistent with a fourfold coordinated aluminum center, completes the expected NMR resonances. The ESI† further contains the obtained IR spectroscopic data.

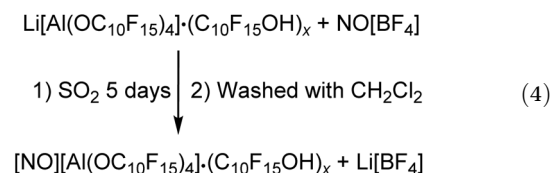**[Ph$_3$C][*pfAd*] (4).** A suitable synthesis protocol to [Ph$_3$C][*pfAd*] (**4**) would allow access to a large number of follow up chemistry. Again, the synthesis as illustrated in eqn (3) was adapted to the already existing protocol for [Ph$_3$C][*pf*] wherein the Li[*pf*] is reacted with Ph$_3$C-Cl in CH$_2$Cl$_2$.[54]

$$\text{Li[Al(OC}_{10}\text{F}_{15}\text{)}_4]\cdot(\text{C}_{10}\text{F}_{15}\text{OH})_x + \text{Ph}_3\text{CCl}$$

$$\text{SO}_2 \downarrow \text{ 5 days}$$

$$[\text{Ph}_3\text{C}][\text{Al(OC}_{10}\text{F}_{15}\text{)}_4]\cdot(\text{C}_{10}\text{F}_{15}\text{OH})_x + \text{LiCl} \qquad (3)$$

$$\downarrow \begin{array}{l}\text{Washed with CH}_2\text{Cl}_2 \\ \text{Crystallized} \\ \text{from } o\text{-DFB}\end{array}$$

$$[\text{Ph}_3\text{C}][\text{Al(OC}_{10}\text{F}_{15}\text{)}_4]$$

However, the Li$^+$ salt used was contaminated with alcohol and is also hardly soluble in CH$_2$Cl$_2$. The reaction started already in the solid state visualized by an immediate color change to yellow after mixing of the starting materials. Addition of the solvent CH$_2$Cl$_2$ resulted in an intense yellow color of the solution indicating the formation of some **4**, yet the large majority remained insoluble at the bottom. The reaction solution was allowed to sediment after two days and analyzed by NMR spectroscopy, showing the presence of the target compound as well as the alcohol C$_{10}$F$_{15}$OH as main compound indicating an incomplete turnover or at least a poor solubility of the target compound in CH$_2$Cl$_2$. Suitable crystals for single-crystal X-ray diffraction (scXRD) were obtained from the reaction mixture after filtration and gas phase diffusion crystallization with *n*-pentane (see X-ray section below). With a yield of less than 3%, this synthesis route does not provide a useful access to [Ph$_3$C][*pfAd*] (**4**). Due to the poor solubility of **4** in CH$_2$Cl$_2$, liquid SO$_2$ was used, and the reaction time was extended to 5 days. Then, the SO$_2$ was removed, the solid washed with CH$_2$Cl$_2$ and crystallized by diffusion crystallization from an *o*-DFB solution with *n*-pentane resulting in a yield of 55% pure **4**. Multinuclear NMR spectroscopy of [Ph$_3$C][*pdAd*] (**4**) in CD$_3$CN shows two resonances in the ^{19}F NMR spectrum at $\delta_F = -122.0$ ppm for the 48 CF$_2$ fluorine atoms and $\delta_F = -223.7$ ppm for the 12 CF fluorine atoms (for details see ESI†). The ^{1}H NMR spectrum of **4** in CD$_3$CN shows the aromatic protons of the trityl cation with chemical shifts of $\delta_H = 7.76$ (*o*-CH), $\delta_H = 7.92$ (*m*-CH) and $\delta_H = 8.33$ ppm (*p*-CH) (for details see ESI†). Interestingly, the trityl signals of the proton NMR spectrum in CD$_3$CN are initially observed as one broad signal. After about 13 h, the signal begins to split and are cleanly resolved after 24 h. The ^{7}Li- and ^{27}Al NMR spectra as well as the IR spectroscopic data (for details see ESI†) confirm the successful synthesis of **4** free of impurities.

[NO][*pfAd*] (5). Commonly used reagents for the introduction of WCAs are the salts of strongly oxidizing agents such as Ag$^+$ and NO$^+$. The higher oxidation potential of NO$^+$ *vs.* ferrocene in CH$_2$Cl$_2$ ($E^0 = 1.40$ V (ref. 34)) compared to Ag$^+$ in CH$_2$Cl$_2$ ($E^0 = 0.77$ V (ref. 34)) enabled the first synthesis of the cation [P$_9$]$^+$.[26] The synthesis of **5** was carried out according to the already published synthesis protocol for [NO][*pf*] with the difference that freshly sublimed NO[BF$_4$] was used as NO$^+$ source instead of NO[SbF$_6$].[55] Li[*pfAd*] (**1**) contaminated with alcohol and NO[BF$_4$] were stirred in SO$_2$ for five days. NO[*pfAd*] (**5**) was isolated from Li[BF$_4$] by filtration and slow removal of the solvent SO$_2$ (eqn (4)).

$$\text{Li[Al(OC}_{10}\text{F}_{15}\text{)}_4]\cdot(\text{C}_{10}\text{F}_{15}\text{OH})_x + \text{NO[BF}_4]$$

$$\downarrow \begin{array}{l}\text{1) SO}_2 \text{ 5 days} \quad \text{2) Washed with CH}_2\text{Cl}_2\end{array} \qquad (4)$$

$$[\text{NO}][\text{Al(OC}_{10}\text{F}_{15}\text{)}_4]\cdot(\text{C}_{10}\text{F}_{15}\text{OH})_x + \text{Li[BF}_4]$$
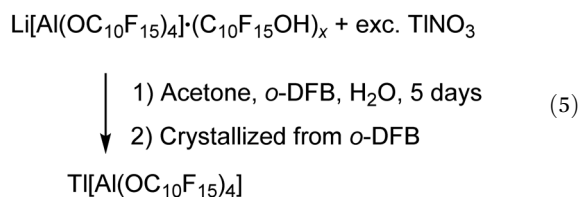
NMR investigations of the isolated solid in CD$_2$Cl$_2$ showed the alcohol as main compound next to the anion. Based on this observation, the alcohol should be washed off with CH$_2$Cl$_2$ in analogy to the [Ph$_3$C][*pfAd*] (**4**) synthesis. Several attempts were unsuccessful and further washing with C$_6$F$_6$ could not remove the alcohol C$_{10}$F$_{15}$OH. Due to the reactivity of the NO$^+$ cation, the choice of potential solvents for purifi-

cation is limited. To the best of our knowledge, it seems likely that there is a strong coordination of the alcohol towards **5**. Furthermore, we cannot provide clear evidence for the presence of the cation NO^+. The NMR spectra (see ESI†) show the already discussed resonances of the anion as well as the alcohol in the ^{19}F NMR spectrum. The absence of a lithium signal confirms the successful metathesis reaction and removal of $Li[BF_4]$. The ^{14}N NMR spectrum shows no signal, which does not necessarily exclude the presence of the NO^+ cation. In fact, the NMR spectra do also not show any signals that would indicate the presence of another cation than NO^+. Typically, the NO^+ cation can be detected by Raman spectroscopy. The Raman spectrum of **5** shows a broad vibrational band at 2332 cm^{-1} of low intensity, which can be assigned to the NO^+ cation. However, the anion has a great influence on the intensity of the NO^+ vibration band of around 2340 cm^{-1}. Thus, $NO[F\text{-}Al(OC(CF_3)_3)_3]$ shows a very intense band, whereas the NO^+ cation in the bridged $[((CF_3)_3CO)_3Al\text{-}F\text{-}Al(OC(CF_3)_3)_3]^-$ anion shows a vibration band of low intensity.[56] Great efforts were therefore made to find suitable crystallization conditions for purification. However, these were unsuccessful. Since there is no clear structural evidence for the NO^+ cation apart from the indications from the Raman spectrum, the obtained compound was investigated for its oxidation capacity. $NO[pfAd]$ (**5**) containing impurities by alcohol and an excess of P_4 were suspended in CH_2Cl_2 under ultrasonic activation resulting in the formation of an orange solution of the known P_9^+ cation in CH_2Cl_2 (for details see ESI†).[26,57] Furthermore, a small amount of ferrocene Fc was added to a solution of **5** in o-DFB resulting in a change of color from orange to blue, indicative for Fc^+ formation. The absence of Li^+ and the further described observations allow the conclusion that the synthesis of $NO[pfAd]$ (**5**) was successful (46%), albeit including a small impurity of the alcohol $C_{10}F_{15}OH$.

Tl[*pfAd*] (**6**). The synthesis of thallium(I) alkoxy aluminate is feasible by reaction of the Li^+ salt with TlF in CH_2Cl_2 in analogy to the preparation of $Ag[Al(OR^F)_4]$ with $(OR^F = OC(CF_3)_3, O(CH)(CF_3)_2)$.[58] However, this reaction showed a strong dependence on the stoichiometry. Any deviation from a 1 : 1 stoichiometry resulted in the formation of $[Tl_3F_2Al(OR^F)_3][Al(OR^F)_4]$ $(OR^F = O(CH)(CF_3)_2)$. Since $Li[pfAd]$ (**1**) contained impurities of the corresponding alcohol and itself is resistant towards air and moisture, the synthesis in this work was carried out with an excess of $TlNO_3$ in a solution of o-DFB, acetone and H_2O (eqn (5)). Here, acetone served as solution intermediary and was allowed to evaporate after a reaction time of 5 d.
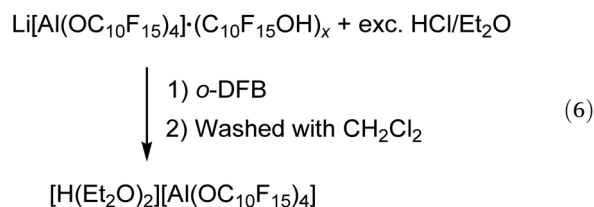
$$Li[Al(OC_{10}F_{15})_4]\cdot(C_{10}F_{15}OH)_x + exc.\ TlNO_3$$

$$\Big\downarrow \begin{array}{l} \text{1) Acetone, }o\text{-DFB, }H_2O\text{, 5 days} \\ \text{2) Crystallized from }o\text{-DFB} \end{array} \quad (5)$$

$$Tl[Al(OC_{10}F_{15})_4]$$

Tl[*pfAd*] (**6**) is well soluble in o-DFB, whereas $TlNO_3$ and $LiNO_3$ show a good solubility in the aqueous phase and consequently could be separated. The obtained colorless solid (65%) showed resonances which indicate the presence of the alcoholate (no alcohol here, ^1H NMR signal of the alcohol at 4.00 ppm is absent) and traces of lithium. Crystals suitable for scXRD were obtained from a solution of **6** in o-DFB solution by gas phase diffusion with n-pentane. While the diffraction data are of very good quality, the model remained unsatisfying (for details see ESI†) but supports the conclusion that Tl[*pfAd*] crystallized without any solvent molecules, neither co-crystallized, nor did the anion coordinate to the Tl^+ cation. Also, the NMR and IR spectroscopic analyses of isolated crystals indicate the target compound to be free of any impurities (for details see ESI†). In addition, this reaction illustrates the high stability of the anion in aqueous environment.

An optimized procedure to clean M[*pfAd*] Salts

The preparation of salts containing the $[pfAd]^-$ anion free of impurities was only possible by derivatization into the $[Ph_3C]^+$ or the Ag^+ salt so far. However, the introduction of the Li^+ and potentially further metal salts was still a declared objective. Hence, we targeted the synthesis of $[H(OEt_2)_2]^+[pfAd]^-$ (**7**) according to eqn (6). Acid **7** should serve as an appropriate starting material for subsequent reactions with $M[N(Si(CH_3)_3)_2]$ (with $M = Li^+, K^+, 0.5\ Mg^{2+}, ...$) under formation of the respective M[*pfAd*] salts.

$$Li[Al(OC_{10}F_{15})_4]\cdot(C_{10}F_{15}OH)_x + exc.\ HCl/Et_2O$$

$$\Big\downarrow \begin{array}{l} \text{1) }o\text{-DFB} \\ \text{2) Washed with }CH_2Cl_2 \end{array} \quad (6)$$

$$[H(Et_2O)_2][Al(OC_{10}F_{15})_4]$$

The synthesis of $[H(OEt_2)_2][pfAd]$ (**7**) was realized by reaction of $Li[pfAd]$ (**1**) containing impurities by alcohol with a solution of HCl in Et_2O (2 M). This reaction is known for the $[pf]^-$ anion with the difference that the preparative effort for **7** was considerably lower due to the simple addition of an excess of etheric HCl solution.[59] The target compound **7** is insoluble in CH_2Cl_2, by contrast to $[H(OEt_2)_2][pf]$. Hence, **7** was extracted with o-DFB. NMR investigations still showed the presence of some traces of $C_{10}F_{15}OH$, which could be washed off with CH_2Cl_2 after which the target compound was obtained pure (for details see ESI†). The ^{19}F- and ^{27}Al NMR spectra show the characteristic signals for the intact counterion, free of impurities. The ^1H NMR spectrum shows the resonances resulting from the CH_2 and CH_3 protons of the coordinating diethyl ether molecules. A broad, downfield-shifted signal at $\delta_H = 16.20$ ppm is observed and can be attributed to the coordinated acidic proton. However, the chemical shift of the acidic proton differs from sample to sample within 4 ppm and depending on the solvent used as already observed for $[H(OEt_2)_2][pf]$.[59] The broad signal exacerbates integration but within the limits of the expected inaccuracies, the consti-

tution of two coordinated diethyl ether molecules per proton can be confirmed. Suitable crystals for scXRD investigations could be obtained from a solution of [H(OEt$_2$)$_2$][*pfAd*] (**7**) in *o*-DFB at −40 °C. Furthermore, we showed that this reaction also works with contaminated Na[*pfAd*] as starting material illustrating the versatility of this reaction (for details see ESI†). The ESI† further contains the obtained IR spectroscopic data for **7**. Starting from **7**, pure

Li[*pfAd*] (**1**) was obtained as etherate by reaction with Li[N(Si(CH$_3$)$_3$)$_2$] = LiHMDS (eqn (7)).

$$[H(Et_2O)_2][Al(OC_{10}F_{15})_4] + LiHMDS$$
$$o\text{-DFB} \downarrow \text{-H(HMDS)} \qquad (7)$$
$$Li[Al(OC_{10}F_{15})_4] \cdot (Et_2O)_2$$
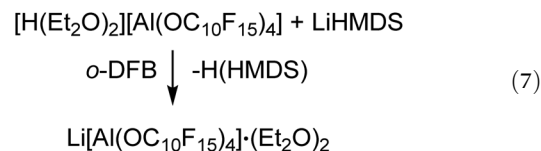
The ^{19}F NMR spectrum only shows the expected resonances attributed to the anion. Nevertheless, the ^{1}H NMR spectrum clearly shows that the obtained Li$^+$-salt is not free of ether (approx. two ether molecules per Li$^+$ salt) even after drying for several hours under reduced pressure at elevated temperatures. Overall, the protonated ether salt **7** can function as a useful starting material for the synthesis of numerous metal salts from commercially available M(HMDS)$_x$ sources.

Outlook to Mg^0-deposition. Reaction of [H(OEt$_2$)$_2$][*pfAd*] (**7**) with Mg(HMDS)$_2$ could deliver solvated Mg[*pfAd*]$_2$, a possible electrolyte salt for Mg^0 deposition, as successfully demonstrated[60] for the related Mg[Al(OCH(CF$_3$)$_2$)$_4$]$_2$. Yet, we recently showed that the position of the LUMO energy of a WCA can highly affect the ability of [Mg(DME)$_3$][WCA] electrolytes for

Table 3 Gibbs free energy $\Delta_r G^{\circ}_{\text{Electronation}}$ for the one-electron reduction of four WCAs and accepting LUMO energy levels for these WCAs in DME (ε_r = 7.30).[52] Except the values for the [pfAd]$^-$ anion, taken from[60] (RI-B3LYP(D3BJ)/def2-TZVPP)

WCA	$\Delta_r G^{\circ}_{\text{Electronation}}$ / [kJ mol^{-1}]	LUMO energy WCA/[eV]
[*pfAd*]$^-$	−131	+0.80
[*pf*]$^-$ (ref. 60)	−53	+3.36
[Al(OCH(CF$_3$)$_2$)$_4$]$^-$ (ref. 60)	+44	+3.42
[B(OCH(CF$_3$)$_2$)$_4$]$^-$ (ref. 60)	−48	+4.17
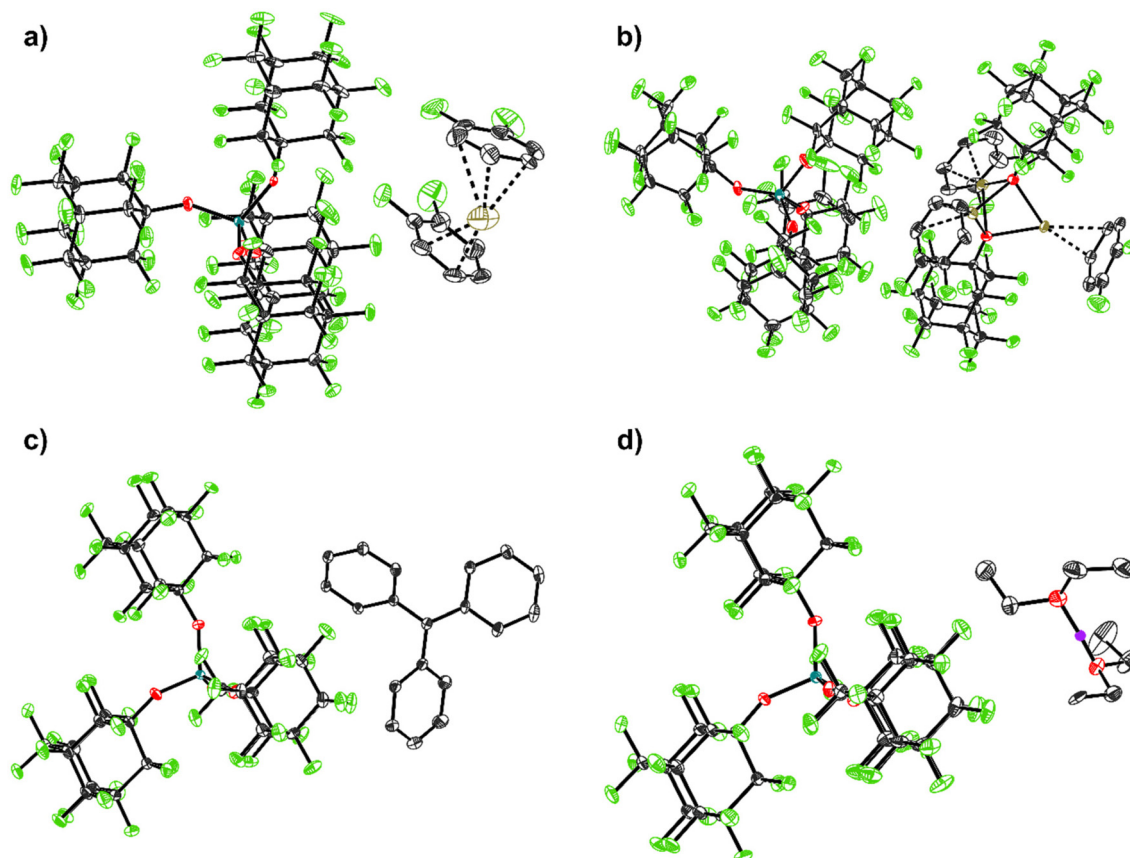
Fig. 2 Molecular structures of the structurally characterized [*pfAd*]$^-$ salts: (a) [Ag(*o*-DFB)$_2$][Al(OC$_{10}$F$_{15}$)$_4$] (2-*o*DFB), (b) [Ag$_3$(OC$_{10}$F$_{15}$)$_2$(*o*-DFB)$_3$][Al(OC$_{10}$F$_{15}$)$_4$] (3), (c) [Ph$_3$C][Al(OC$_{10}$F$_{15}$)$_4$] (4), (d) [H(OEt$_2$)$_2$][Al(OC$_{10}$F$_{15}$)$_4$] (7). Hydrogen atoms are omitted for clarity with the exception for the acidic, bridging proton in (d) (purple). Disorders are omitted for clarity for (a) and (b) as well as two further *o*-DFB molecules with an occupation number of 4% in (b). The main occupation numbers are presented here. Thermal displacement ellipsoids were drawn at the 50% probability level. For details see ESI.†

Mg^0 deposition.[60] Apparently, perfluorinated WCAs like $[pf]^-$ can accept an electron from the negative Mg electrode, form the radical dianion $[WCA]^{•2-}$, decompose with liberation of fluoride ions that combine with the Mg^{2+} ions from the electrolyte to give insulating Rutile-structured MgF_2 and prevent Mg^0 deposition. Hence, the LUMO energies as well as the Gibbs energy for the electronation reaction of four WCAs in solution ($[WCA]^- + e^- \rightarrow [WCA]^{•2-}$) were calculated with inclusion of the COSMO solvation model for 1,2-dimethoxyethane.

The LUMO energy of the $[pfAd]^-$ anion is the lowest in Table 3 and consequently also the calculated $\Delta_r G^{\circ}_{Electronation}$ clearly shows that the electronation of the $[pfAd]^-$ anion (as well as $[pf]^-$) are thermodynamically feasible in solution. Based on these results and the observed suppressed Mg^0 deposition with the $[pf]^-$ anion, but **not** with the related $[Al(OCH(CF_3)_2)_4]^-$ for which $\Delta_r G^{\circ}_{Electronation}$ is endergonic,[60] we suggest that Mg^0 deposition will be unlikely with WCA-electrolytes containing major (per-)fluorinated entities such as the $[pfAd]^-$ anion, as their tendency towards electronation is too high.

Molecular structures of the [pfAd] Salts

[Ag(o-DFB)₂][pfAd] (2-oDFB). When Ag[pfAd] (2) was dissolved in o-DFB and crystallized by gas phase diffusion with n-pentane, colorless, block-shaped crystals were obtained. In the molecular structure, the Ag^+ cation is coordinated by two o-DFB molecules in a disordered fashion, exhibiting both η^2- and η^3-coordination (see Fig. 2(a)). In the structure of [Ag(o-DFB)₂][pfAd] (2-oDFB), also the silver atom is disordered and had to be described by three PARTs (occupancies of 0.674, 0.232 and 0.094). A very similar disorder was observed for this cation when crystallized with the $[pf]^-$ anion.[56] Also the anion is disordered in both structures. In 2-oDFB, three of the four $OC_{10}F_{15}$ ligands are disordered (with occupancies of ca. 0.6 and 0.4 for all of them). Due to the strong disorder, we refrain from discussing bond lengths and angles in the anion.

[Ag₃(OC₁₀F₁₅)₂(o-DFB)₃][pfAd] (3). When Ag[pfAd] (2), which was contaminated with Ag[OC₁₀F₁₅], was dissolved in o-DFB and crystallized by gas phase diffusion with n-pentane, colorless needles were obtained. In the molecular structure, three silver atoms and two $OC_{10}F_{15}$ moieties form a trigonal bipyramidal $[Ag_3(OC_{10}F_{15})_2]^+$ cluster cation in which the three silver atoms span the triangular basis (Fig. 2(b)). The perfluoro-adamantanoxy ligands coordinate to all three silver atoms through their oxygen atoms. Each Ag^+ is coordinatively saturated by binding to one o-DFB molecule. A closely related cation is found in the salt $[(AgL)_3(OR^F)_2][pf]$ that formed by the reaction of Ag[pf] with 2 eq. of Ag(OC(CF₃)₃) in the presence of L = C_2H_4 or i-C_4H_8.[61] A discussion of the molecular structure is prohibited due to the strong disorder, but the chemical composition is clearly confirmed. The result highlights that the alcohol needs to be sublimed after drying over molecular sieves prior to use in anion synthesis.
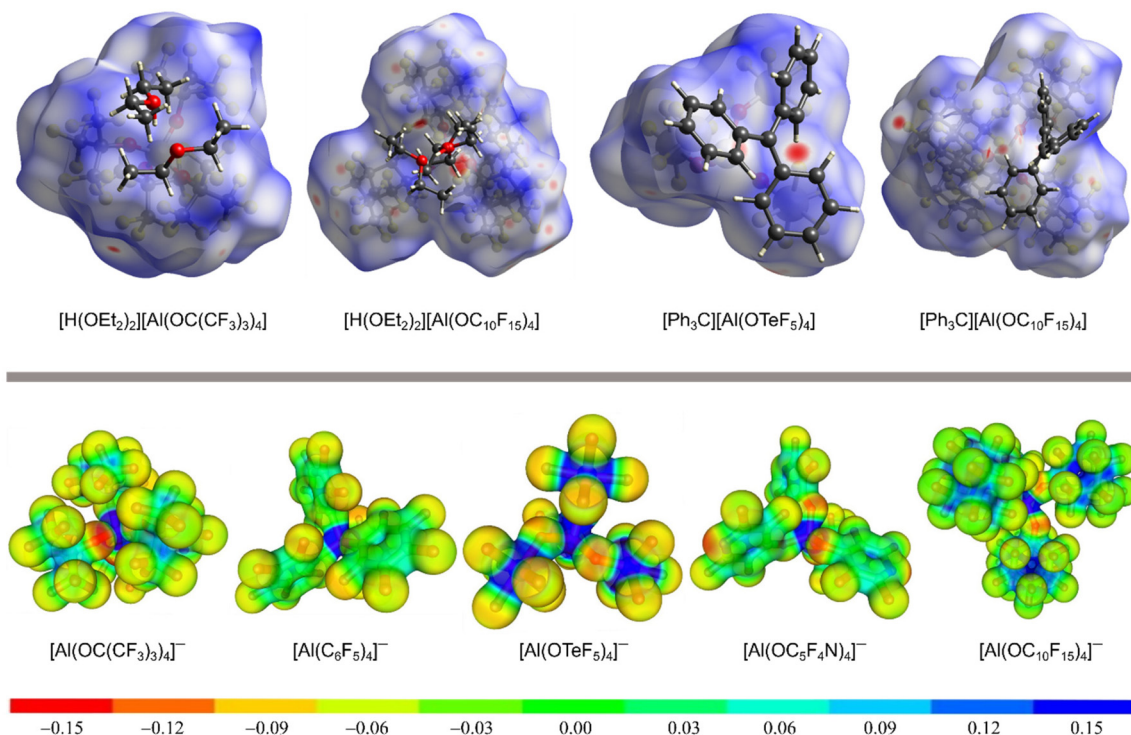

Fig. 3 Top: Hirshfeld surface analysis of [H(OEt₂)₂][WCA] (with WCA = $[pf]^-$ ref. 59) and $[pfAd]^-$) and [Ph₃C][WCA] (with WCA = $[Al(OTeF_5)_4]^-$ (ref. 31) and $[pfAd]^-$).[63] The red colored areas show close cation–anion contacts below the van der Waals radii, whereas blue colored areas indicated distances above the van der Waals radii. Bottom: Projection of the BB86(D3BJ)/def-SV(P) calculated electrostatic potential mapped onto a 0.025 e⁻ Bohr⁻³ isodensity surface of the $[pfAd]^-$ anion in comparison to already known WCAs.

[Ph₃C][*pfAd*] (4). When a solution of **4** in CH_2Cl_2 was crystallized by gas phase diffusion with *n*-pentane, yellow, block-shaped crystals could be grown, which were suitable for scXRD. The molecular structure is shown in Fig. 2(c). As expected, the trityl cation $[Ph_3C]^+$ exhibits a three bladed propeller structure, and the central C atom is surrounded by the *ipso* carbon atoms of the phenyl rings in a planar fashion (sum of angles 360.01(14)°). The shortest F–H distance (between anion and cation) is 247.8 pm, which is longer than expected for any halogen-hydrogen bonding.[62] The shortest distance between the central carbon of the trityl cation and any fluorine atom of the anion is 456.3(3) pm and thus much longer than the sum of the van der Waals radii. Further, the molecular structure does not show any signs of disorder, and thus, a structural discussion of the anion is possible. Within the $[pfAd]^-$ anion, the O–Al–O angle amounts to ideal 109.47 (8)° on average (ranging from 106.92(6)° to 111.68(7)°). The Al–O–C bond angles range from 147.6(1)° to 150.8(1)° (avg. 149.2(1)°), the Al–O distances from 172.4(2) pm to 173.7(2) pm (avg. 173.0(2) pm) and the O–C distances from 134.5(2) pm to 134.9(2) pm (avg. 134.7(2) pm). These values closely resemble those of the $[pf]^-$ WCA.

[H(OEt₂)₂][*pfAd*] (7). Crystals suitable for scXRD were obtained by storage of a solution of **7** in *o*-DFB at −40 °C. The molecular structure is shown in Fig. 2(d). Also in this structure, the anion is not disordered, thus allowing for a structural discussion. The O–Al–O angles range from 107.48(12)° to 111.65(12)° (avg. 109.5(1)°) and the Al–O–C bond angles from 147.3(2)° to 148.9(2)° (avg. 148.0(2)°). The Al–O distances range from 172.7(2) pm to 173.0(2) pm (avg. 172.8(2) pm) and the O–C distances from 134.5(4) pm to 135.4(4) pm (avg. 135.0 (4) pm). The $[H(OEt_2)_2]^+$ cation is disordered (64 : 36 ratio) and shows the typical O–O separation of 245.1(12) pm within the major PART (for details see ESI†).

The delocalization of the negative charge in WCAs should reduce the overall cation–anion interaction. Fig. 3 visualizes the coordination ability of the $[pfAd]^-$ anion in comparison to other well-known WCAs. The first row of Fig. 3 shows Hirshfeld surface analyses of salts of the $[pfAd]^-$ anion in comparison to salts of the WCAs $[pf]^-$ (ref. 59) and $[Al(OTeF_5)_4]^-$.[31] Fig. 3 shows several red areas indicating cation–anion distances below the van der Waals radii, most visible for the salt $Ph_3C^+[Al(OTeF_5)_4]^-$. Yet, overall the Hirshfeld surfaces of the WCAs indicate very well dispersed and only little interacting surface sites. The coordination ability of WCAs can further be visualized by a projection of the BP86(D3BJ)/def-SV(P) calculated electrostatic potential onto a $0.025\ e^-\ Bohr^{-3}$ isodensity surface, shown in the bottom row of Fig. 3. A red coloration indicates a high accumulation of negative charge. The charge in the $[pfAd]^-$ anion is strongly delocalized resulting in only faintly red colored oxygen and almost green fluorine atoms. In contrast, the oxygen atoms in the anions $[pf]^-$ and $[Al(OC_5F_4N)_4]^-$ are more red colored and show a higher electron density. Furthermore, Fig. 3 shows that a lower number of fluorine atoms reduces the delocalization of the negative charge and results in a higher electron density on the fluorine atoms, see for example on $[Al(OTeF_5)_4]^-$.

Conclusions

Quantum chemical calculations of the novel weakly coordinating anion $[Al(OC_{10}F_{15})_4]^-$ $[pfAd]^-$ allude an improved stability towards reactive cations compared to the widely used $[Al(OC(CF_3)_3)_4]^-$ $[pf]^-$ anion. The $[pfAd]^-$ anion is featured by a high fluoride ion affinity of the corresponding Lewis acid, ligand affinity as well as a high stability towards proton and copper induced decomposition. Unexpectedly, the development of rational synthesis routes to starting materials to introduce the anion was challenging. The synthesis of Li[*pfAd*] was always accompanied by the occurrence of unreacted alcohol, which cannot be removed, nor omitted. This crucial problem was solved in subsequent salt metathesis reactions enabling the syntheses and structural characterizations of the pure Ag^+, Ph_3C^+ and $[H(OEt_2)]^+$ salts in good to excellent yields. Especially the protonated ether salt allows an easy access to a variety of useful materials by further reaction with M[N(Si(CH₃)₃)₂], which was exemplarily demonstrated here by the reaction with Li[N(Si(CH₃)₃)₂] finally providing access to a pure, but ether solvated Li[*pfAd*] salt. The useful water stability of the $[pfAd]^-$ anion is highlighted by the synthesis of Tl[*pfAd*] under aqueous reaction conditions. This facilitates further application enormously. The actual synthetic value of the $[pfAd]^-$ anion to stabilize strong electrophiles is currently under investigation.

Experimental and method section

General considerations

All manipulations were carried out under an inert argon atmosphere, using standard vacuum and Schlenk techniques or a glovebox (box atmosphere kept below 1 ppm H_2O/O_2) unless stated otherwise. Glassware has been stored in an oven at 180 °C overnight and was further dried with a heat gun under vacuum prior to use. Unless stated otherwise all reactions were performed in special double-Schlenk tubes separated by a G3 or G4 frit and equipped with grease-free PTFE or glass valves. All solvents and reagents were dried using conventional drying agents, distilled afterwards and stored under argon atmosphere over activated 3 Å molecular sieves.

NMR spectroscopy

NMR spectra were recorded on a Bruker Avance II⁺ 400 MHz WB, Bruker Avance III HD 300 MHz and a Bruker Avance DPX 200 MHz NMR spectrometer at room temperature (unless described otherwise). The software package Bruker TopSpin 4.0.7 was used for analysis. The spectra were calibrated based on the chemical shift of the solvents used. All relevant spectra can be found in the ESI.†

Vibrational spectroscopy

Raman spectroscopy was performed at r.t. with a Bruker VERTEX 70 spectrometer equipped with a Bruker RAM II module (Nd/YAG 1064 nm laser) with a nitrogen cooled Ge

detector. The samples were measured in sealed soda-lime glass Pasteur pipettes or in NMR tubes equipped with a gastight J. Young valve in the region of 4000 to 200 cm^{-1} with a resolution of 4 cm^{-1} with 1000 scans. ATR FTIR spectroscopy was performed at r.t. with a diamond crystal on a Bruker ALPHA spectrometer with a QuickSnap Platinum ATR sampling module inside an inert atmosphere glovebox. A KBr beam splitter was used for the spectral range from 4000 to 400 cm^{-1}. The spectra were recorded with 64 scans and resolution of 2 cm^{-1}. Data processing was carried out with the software package OPUS 7.5 and OriginPro 2019b. Unless stated differently, the usual processing procedure included a baseline correction with one iteration and a standardization of the signal intensities. The relative band intensities were described as follows: ≥0.8 = very strong (vs), ≥0.6 = strong (s), ≥0.4 = medium (m), ≥0.2 = weak (w), <0.2 = very weak (vw).

Single crystal X-ray diffraction

Single-crystal X-ray data were collected on a Bruker SMART APEXII QUAZAR three-circle diffractometer with a microfocus sealed X-ray tube using Incoatec mirror optics as a monochromator. Mo-K$_\alpha$ radiation (λ = 0.71073 Å) was used for all measurements. The obtained crystals were coated with perfluoropolyalkylether oil (AB128330, ABCR GmbH & Co. KG), mounted on 0.1 to 0.3 mm micromounts and shock-cooled to 100 K on the diffractometer (using an Oxford Cryosystem open flow N$_2$ cooling device).[64] All data were integrated with SAINT,[65] a multi-scan absorption-correction using SADABS-2016/2 was applied.[66] The structures were solved by direct methods using SHELXT 2014/5[67] and refined by full-matrix least-squares methods against F^2 by SHELXL-2018/3[68] employing the shelXle GUI (Revision 1449).[69] All non-hydrogen atoms were refined with anisotropic displacement parameters. The hydrogen atoms were refined isotropically on calculated positions using a riding model with their U_{iso} values constrained to 1.5 times the U_{eq} of their pivot atoms for terminal sp^3 carbon atoms and 1.2 times for all other carbon atoms. Disordered moieties were refined using bond-length restraints and displacement-parameter restraints. Some parts of the disorder model were introduced by the program DSR.[36,37] The cif files were generated using FinalCif.[37,70] Graphical representations were prepared using the software OLEX2 (version 1.3.0).[71] Crystallographic data (including structure factors) for the structures reported in this paper have been deposited with the Cambridge Crystallographic Data Centre. CCDC 2224626 (for **2**-*o*DFB), 2224627 (for **3**), 2224628 (for **4**), 2224629 (for **7**)† contain the supplementary crystallographic data for this paper. Additionally, the cif file of Tl[Al(OC$_{10}$F$_{15}$)$_4$] is attached (including structure factors) since it was not deposited with the CCDC.†

Computational details

Unless stated otherwise, quantum chemical calculations were carried out with the TURBOMOLE software[72] (v7.2 or v7.5) in the highest possible point group using the DFT functional BP86[73] or pbeh-3c[74] (the resolution-of-identity RI approxi-

mation[75]) in combination with the def-SV(P),[76] def2-mSVP[74] and def-TZVPP[77] basis sets and D3 dispersion correction with Becke–Johnson (BJ) damping,[39,40] a fine integration grid (m3 or m4) and the default SCF convergence criteria (10^{-6} a.u.). Every species presented herein was checked in terms of reasonable geometry and electronic occupation with the EIGER module. Vibrational frequencies were calculated analytically using the AOFORCE module.[78] All structures represented true minima without imaginary frequencies on the respective hypersurface. Thermodynamic terms were calculated with inclusion of zero-point energy and thermal contributions to the enthalpy/entropy (FREEH tool; unscaled BP86 vibrational frequencies). Gibbs free energies of solvation were calculated with the COSMO model.[79] Single point calculations at the DLPNO-CCSD(T)[80]/cc-pVQZ[81] and DSD-PBEP86(D3BJ)[82]/def2-QZVPP[83] level of theory were performed with ORCA (v4.1.2 or v5.0.2) based on the pbeh-3c structures. The ESI† contains a more detailed description of all performed calculations.

Preparation of Li[Al(OC$_{10}$F$_{15}$)$_4$]·(C$_{10}$F$_{15}$OH)$_x$ (with x = 0.43)

Purified and slightly ground colorless (!) LiAlH$_4$ (0.100 g, 2.64 mmol) and perfluoro-1-adamantanol (5.005 g, 11.86 mmol, 4.50 eq.) were weighed into a Schlenk flask and suspended in *o*-DFB (40 mL). The reaction mixture was stirred for 3 h under reflux. The solvent was removed under reduced pressure, the obtained colorless solid was washed with toluene (3×, 20 mL), dried under reduced pressure at 100 °C for 3 h (4.80 g, 2.53 mmol, 96%) and analyzed by NMR spectroscopy showing the impurity of unreacted alcohol C$_{10}$F$_{15}$OH (Li[Al(OC$_{10}$F$_{15}$)$_4$] : C$_{10}$F$_{15}$OH = 1.0 : 0.43 by integration of the CF groups) (Note: The chemical shift of the proton resonance of the OH group of C$_{10}$F$_{15}$OH shows a significant downfield shift in THF compared to the same signal in *o*-DFB. The yield was determined by use of the calculated molar mass of 1891.74 g mol^{-1} for Li[Al(OC$_{10}$F$_{15}$)$_4$]·(C$_{10}$F$_{15}$OH)$_x$ with x = 0.43). ^{1}H NMR (300.18 MHz, 298 K, THF): δ = 9.58 (br. s, 1H, C$_{10}$F$_{15}$OH) ppm. ^{7}Li NMR (116.66 MHz, 298 K, THF): δ = −0.5 (s, 1Li, Li[Al(OC$_{10}$F$_{15}$)$_4$]) ppm. ^{19}F NMR (282.45 MHz, 298 K, THF): δ = −224.0 (m, CF, 12F, Li[Al(OC$_{10}$F$_{15}$)$_4$]), −223.4 (m, CF, 3F, C$_{10}$F$_{15}$OH), −140.2 (m, CF, 2F, *o*-DFB), −122.0 (m, CF$_2$, 48F, Li[Al(OC$_{10}$F$_{15}$)$_4$]), −121.8 (chemical shift not exactly determinable due to overlapping, CF$_2$, 12F, C$_{10}$F$_{15}$OH) ppm. ^{27}Al NMR (78.22 MHz, 298 K, THF): δ = 34.6 (s, 1Al, Li[Al(OC$_{10}$F$_{15}$)$_4$]) ppm.

Preparation of Na[Al(OC$_{10}$F$_{15}$)$_4$] containing impurities by C$_{10}$F$_{15}$OH

Purified and slightly ground NaAlH$_4$ (0.033 g, 0.61 mmol) and perfluoro-1-adamantanol (1.074 g, 2.544 mmol, 4.16 eq.) were weighed into a Schlenk flask and suspended in *o*-DFB (10 mL). The reaction mixture was stirred for two days under reflux and analyzed by NMR spectroscopy. The solvent was removed under reduced pressure, washed with toluene (3× 5.0 mL) and dried *in vacuo* at 90 °C. The obtained colorless solid (0.980 g, 0.565 mmol, 92.5%) was analyzed by NMR spectroscopy showing impurity of unreacted alcohol C$_{10}$F$_{15}$OH and very

small amounts of $[F-Al(OC_{10}F_{15})_3]^-$. ^1H NMR (300.18 MHz, 298 K, o-DFB/THF): δ = 9.52 (br. s, 1H, $C_{10}F_{15}OH$) ppm. ^{19}F NMR (282.45 MHz, 298 K, o-DFB/THF): δ = −223.7 (m, CF, 12F, $Na[Al(OC_{10}F_{15})_4]$), −223.2 (m, CF, 3F, $C_{10}F_{15}OH$), −191.3 (m, F, 1F, $[F-Al(OC_{10}F_{15})_3]^-$), −122.2 (m, CF_2, 12F, $C_{10}F_{15}OH$), −121.7 (m, CF_2, 48F, $Na[Al(OC_{10}F_{15})_4]$) ppm. ^{23}Na NMR (79.40 MHz, 298 K, o-DFB/THF): δ = −6.5 (s, 1Na, $Na[Al(OC_{10}F_{15})_4]$) ppm. ^{27}Al NMR (78.22 MHz, 298 K, o-DFB/THF): δ = 34.9 (s, 1Al, $Na[Al(OC_{10}F_{15})_4]$), 42.5 (broad, 1Al, $[F-Al(OC_{10}F_{15})_3]^-$) ppm.

Preparation of $Ag[Al(OC_{10}F_{15})_4]$ containing impurities by $C_{10}F_{15}O^-$

$Li[Al(OC_{10}F_{15})_4]$ (0.205 g, 0.152 mmol) containing impurities of the alcoholate $C_{10}F_{15}O^-$ (since this was one of the first attempts wherein the dried alcohol $C_{10}F_{15}OH$ was not sublimed prior to synthesis of $Li[Al(OC_{10}F_{15})_4]$ consequently containing $NaOC_{10}F_{15}$) and AgF (0.048 g, 0.378 mmol, 3.17 eq.) were suspended in o-DFB (5.0 mL) and sonicated for 14 h. After sedimentation of the solid an NMR was measured from the solution. The reaction mixture was filtered and crystallized by diffusion crystallization with n-pentane (5 mL) for purification. Two different sorts of crystals suitable for single crystal XRD were obtained as colorless needles ($[Ag_3(OC_{10}F_{15})_2(o\text{-}DFB)_3][Al(OC_{10}F_{15})_4]$) (3) and colorless blocks ($[Ag(o\text{-}DFB)_2][Al(OC_{10}F_{15})_4]$) (2-oDFB). Since it was impossible to separate the two different sorts of crystals, the declaration of a yield is not reasonable at this point. For further investigation, an NMR spectrum of the isolated crystals containing both sorts of crystals was measured in CD_2Cl_2 containing undissolved solid. ^1H NMR (400.17 MHz, 298 K, CD_2Cl_2): δ = 7.13 (m, 2H, o-DFB), 7.19 (m, 2H, o-DFB) ppm. ^{19}F NMR (376.54 MHz, 298 K, CD_2Cl_2): δ = −223.3 (m, CF, 12F, $Ag[Al(OC_{10}F_{15})_4]$), −222.4 (m, CF, 3F, $AgOC_{10}F_{15}$), −139.4 (m, 2F, o-DFB), −122.6 (m, CF_2, 12F, $AgOC_{10}F_{15}$), −121.6 (m, CF_2, 48F, $Ag[Al(OC_{10}F_{15})_4]$) ppm. ^{27}Al NMR (104.27 MHz, 298 K, CD_2Cl_2): δ = 35.0 (s, 1Al, $Ag[Al(OC_{10}F_{15})_4]$) ppm.

Preparation of pure $Ag(CH_2Cl_2)_2[Al(OC_{10}F_{15})_4]$

$Li[Al(OC_{10}F_{15})_4]$ (0.855 g, 0.498 mmol) containing impurities of the alcohol $C_{10}F_{15}OH$ and AgF (0.104 g, 0.820 mmol, 1.65 eq.) were suspended in o-DFB (3.0 mL) and sonicated for 10 h. The solvent o-DFB was removed under reduced pressure. CH_2Cl_2 (3.0 mL) was added, and the target compound was extracted 5 times by condensing the solvent back to the reaction mixture after filtration. n-pentane was added into the empty part of the H-cell (where the reaction took place) for diffusion crystallization. The target compound was obtained as colorless crystals (0.360 g, 0.200 mmol, 40%), washed with n-pentane (2× 5 mL), dried under reduced pressure, and analyzed by NMR spectroscopy. ^{19}F NMR (282.45 MHz, 298 K, CD_2Cl_2): δ = −223.4 (m, CF, 12F, $Ag[Al(OC_{10}F_{15})_4]$), −122.0 (m, CF_2, $Ag[Al(OC_{10}F_{15})_4]$), −121.6 (m, CF_2, $Ag[Al(OC_{10}F_{15})_4]$) ppm. ^{27}Al NMR (78.22 MHz, 298 K, CD_2Cl_2): δ = 34.7 (s, 1Al, $Ag[Al(OC_{10}F_{15})_4]$) ppm. FTIR (Diamant, ATR): $\tilde{\nu}$ = 2966 (vw), 1351 (vw), 1268 (vs), 1106 (vw), 1038 (vw), 981 (m), 955 (vs), 852 (vw), 814 (vw), 758 (vw), 736 (vw), 679 (vw), 651 (vw), 533 (vw), 442 (vw), 402 cm^{-1}.

Preparation of $[Ph_3C][Al(OC_{10}F_{15})_4]$

$Li[Al(OC_{10}F_{15})_4]$ (0.260 g, 0.152 mmol) containing impurities of the alcohol $C_{10}F_{15}OH$ and Ph_3CCl (0.067 g, 0.240 mmol, 1.59 eq.) were suspended in SO_2 (3.0 mL) and stirred at room temperature for six days. The reaction mixture was allowed to sediment and filtered afterwards. The sedimented solid was extracted five times by condensing SO_2 back, stirring and filtration resulting in an intensive yellow solution on product side and a colorless solid on reactant side. SO_2 was removed under reduced pressure. The yellow solid was washed with CH_2Cl_2 (5.0 mL) in order to remove impurities since the target compound is hardly soluble in CH_2Cl_2. The solid residue was dissolved in o-DFB (2.0 mL) and crystallized by diffusion crystallization with n-pentane (30 mL) for purification (Note: The progress of crystallization could be very well traced by the decolorization of the initially bright yellow solution). The yellow crystals (0.164 g, 0.084 mmol, 55%; Note: 65% yield considering that the used $Li[Al(OC_{10}F_{15})_4]$ was contaminated by 0.73 eq. alcohol) were isolated after filtration and characterized by NMR spectroscopy. The discussed molecular structure was obtained from a previous attempt, where CH_2Cl_2 was used as solvent. Diffusion crystallization with n-pentane resulted in the formation of yellow crystals. ^1H NMR (200.13 MHz, 298 K, CD_3CN): δ = 7.76 (d, o-CH, 6H, $[Ph_3C]^+$), 7.92 (t, m-CH, 6H, $[Ph_3C]^+$), 8.33 (t, p-CH, 3H, $[Ph_3C]^+$) ppm. ^7Li NMR (116.66 MHz, 298 K, CD_3CN): δ = −2.7 (br. S, 1Li, Li^+, only traces) ppm. ^{13}C NMR (50.32 MHz, 298 K, CD_3CN): δ = 130.2 (s, Ph, $[Ph_3C][Al(OC_{10}F_{15})_4]$, 140.2 (s, Ph, $[Ph_3C][Al(OC_{10}F_{15})_4]$, 143.1 (s, Ph, $[Ph_3C][Al(OC_{10}F_{15})_4]$, 143.2 (s, Ph, $[Ph_3C][Al(OC_{10}F_{15})_4]$, 212.1 (s, $C^{carbenium}$, $[Ph_3C][Al(OC_{10}F_{15})_4]$ ppm. ^{19}F NMR (282.45 MHz, 298 K, CD_3CN): δ = −223.7 (m, CF, 12F, $[Ph_3C][Al(OC_{10}F_{15})_4]$), −122.0 (m, CF_2, 48F, $[Ph_3C][Al(OC_{10}F_{15})_4]$) ppm. ^{27}Al NMR (78.22 MHz, 298 K, CD_3CN): δ = 34.8 (s, 1Al, $[Ph_3C][Al(OC_{10}F_{15})_4]$) ppm. FTIR (Diamant, ATR): $\tilde{\nu}$ = 1585 (w), 1486 (vw), 1454 (vw), 1360 (w), 1293 (w), 1269 (vs), 1189 (vw), 1105 (vw), 978 (m), 955 (vs), 843 (vw), 807 (vw), 767 (vw), 756 (vw), 704 (vw), 678 (vw), 650 (vw), 624 (vw), 609 (vw), 533 (vw), 467 (vw), 441 (vw), 402 (vw) cm^{-1}.

Preparation of $[NO][Al(OC_{10}F_{15})_4]$ containing impurities by $C_{10}F_{15}OH$

$Li[Al(OC_{10}F_{15})_4]$ (0.304 g, 0.177 mmol) containing impurities by alcohol $C_{10}F_{15}OH$ and $[NO][BF_4]$ (0.025 g, 0.214 mmol, 1.21 eq.) were suspended in SO_2 (3.0 mL) and stirred for 4 d at r.t. The reaction mixture was allowed to sediment and filtered. The solid residue was extracted once by condensing SO_2 back followed by filtration. SO_2 was removed under reduced pressure and the orange solid residue was washed with C_6F_6 (2.5 mL). The solvent was removed and the solid residue dried under reduced pressure and the target compound obtained as orange solid (0.143 g, 0.082 mmol, 46%) containing impurities of the alcohol. ^1H NMR (400.17 MHz, 298 K, o-DFB): δ = 4.09 (m, 1H, $C_{10}F_{15}OH$) ppm. ^{19}F NMR (376.54 MHz, 298 K, o-DFB):

$\delta = -223.2$ (m, CF, 12F, [NO][Al(OC$_{10}$F$_{15}$)$_4$]), -222.8 (m, CF, 3F, C$_{10}$F$_{15}$OH), -163.6 (m, 6F, C$_6$F$_6$), -121.5 (m, CF$_2$, 12F, C$_{10}$F$_{15}$OH), -121.3 (m, CF$_2$, 48F, [NO][Al(OC$_{10}$F$_{15}$)$_4$]) ppm. ^{27}Al NMR (104.27 MHz, 298 K, o-DFB): $\delta = 35.4$ (s, 1Al, [NO][Al(OC$_{10}$F$_{15}$)$_4$]) ppm. FT-Raman: $\tilde{\nu} = 2332$ (vw), 1292 (m), 1148 (vw), 727 (vw), 700 (vw), 667 (vw), 630 (vw), 573 (w), 500 (vw), 442 (w), 403 (vs), 372 (vs), 311 (s) cm^{-1}.

Preparation of [P$_9$][Al(OC$_{10}$F$_{15}$)$_4$] containing impurities by C$_{10}$F$_{15}$OH

[NO][Al(OC$_{10}$F$_{15}$)$_4$] (0.060 g, 0.034 mmol, containing impurities by alcohol C$_{10}$F$_{15}$OH) and P$_4$ (0.011 g, 0.089 mmol, 2.60 eq.) were weighed into a J. Young valve NMR tube. After addition of CH$_2$Cl$_2$ (0.5 mL) the reaction mixture was sonicated for 20 h. A yellow solution containing also undissolved solid was obtained and analyzed by NMR spectroscopy. ^{1}H NMR (200.13 MHz, 298 K, CH$_2$Cl$_2$): $\delta = 3.94$ (br. s, 1H, C$_{10}$F$_{15}$OH) ppm. ^{19}F NMR (188.31 MHz, 298 K, CH$_2$Cl$_2$): $\delta = -223.6$ (m, CF, 12F, [P$_9$][Al(OC$_{10}$F$_{15}$)$_4$]), -222.5 (m, CF, 3F, C$_{10}$F$_{15}$OH), -121.9 (m, CF$_2$, [P$_9$][Al(OC$_{10}$F$_{15}$)$_4$]), -121.5 (m, CF$_2$, [P$_9$][Al(OC$_{10}$F$_{15}$)$_4$]), -121.1 (m, CF$_2$, 12F, C$_{10}$F$_{15}$OH) ppm. ^{31}P NMR (81.01 MHz, 298 K, CH$_2$Cl$_2$): $\delta = -522.1$ (s, 4P, P$_4$), -247.3 (m, 4P, [P$_9$]$^+$, P$_C$, [P$_2$P$_2$PP$_2$'P$_2$']$^+$), 61.4 (m, 1P, [P$_9$]$^+$, P$_B$, [P$_2$P$_2$PP$_2$'P$_2$']$^+$), 110.5 (m, 4P, [P$_9$]$^+$, P$_A$, [P$_2$P$_2$PP$_2$'P$_2$']$^+$) ppm.

Preparation of Tl[Al(OC$_{10}$F$_{15}$)$_4$] containing impurities by C$_{10}$F$_{15}$OH/C$_{10}$F$_{15}$O$^-$

Li[Al(OC$_{10}$F$_{15}$)$_4$] (0.610 g, 0.355 mmol) containing impurities by alcohol C$_{10}$F$_{15}$OH and TlNO$_3$ (0.209 g, 0.785 mmol, 2.21 eq.) were dissolved in o-DFB (6.0 mL), acetone (0.5 mL) and H$_2$O (0.5 mL) and stirred at room temperature overnight. Additional H$_2$O (20 mL) was added to dissolve the precipitated colorless solid. The reaction solution was sonicated for 4 h. The organic phase was separated, washed with H$_2$O (3× 5 mL) and the solvents were removed under reduced pressure. The obtained colorless solid (0.442 g, 0.231 mmol, 65%) was analyzed by NMR spectroscopy showing impurities by alcoholate and only traces of Li$^+$. The colorless solid was dissolved in o-DFB (1.5 mL) and crystallized with n-pentane. Initially, only amorphous solid precipitated, but after another few days, the formation of crystals could be observed, which were examined by NMR spectroscopy and single crystal X-ray diffraction. Since the obtained crystals are embedded in the amorphous solid, it was hard to separate larger amounts of crystals from the rest and therefore this is not a suitable purification method. NMR data before crystallization: ^{1}H NMR (400.17 MHz, 298 K, o-DFB): $\delta = 2.31$ (br. s, 6H, acetone) ppm. ^{7}Li NMR (155.52 MHz, 298 K, o-DFB): $\delta = 2.1$ (Li$^+$, only traces, LiOC$_{10}$F$_{15}$ or Li[Al(OC$_{10}$F$_{15}$)$_4$]) ppm. ^{19}F NMR (282.45 MHz, 298 K, o-DFB): $\delta = -223.2$ (m, CF, 12F, Tl[Al(OC$_{10}$F$_{15}$)$_4$]), -222.8 (m, CF, 3F, C$_{10}$F$_{15}$OH/C$_{10}$F$_{15}$O$^-$), -121.3 (m, CF$_2$, 48F, Tl[Al(OC$_{10}$F$_{15}$)$_4$]) ppm. ^{27}Al NMR (78.22 MHz, 298 K, o-DFB): $\delta = 35.4$ (s, 1Al, Tl[Al(OC$_{10}$F$_{15}$)$_4$]) ppm. NMR Data after crystallization: ^{1}H NMR (400.17 MHz, 298 K, CD$_2$Cl$_2$): $\delta = 2.15$ (br. s, 6H, acetone) ppm. ^{7}Li NMR (155.52 MHz, 298 K, CD$_2$Cl$_2$): no signal. ^{19}F NMR (376.54 MHz, 298 K, CD$_2$Cl$_2$): $\delta = -223.4$ (m, CF, 12F, Tl[Al(OC$_{10}$F$_{15}$)$_4$]), -121.8 (m, CF$_2$, 48F, Tl[Al(OC$_{10}$F$_{15}$)$_4$]) ppm. ^{27}Al NMR (104.27 MHz, 298 K, CD$_2$Cl$_2$): $\delta = 34.7$ (s, 1Al, Tl[Al(OC$_{10}$F$_{15}$)$_4$]) ppm. FTIR (Diamant, ATR): $\tilde{\nu} = 1697$ (vw), 1686 (vw), 1350 (vw), 1292 (w), 1268 (vs), 1109 (vw), 979 (s), 954 (vs), 762 (vw), 678 (w), 651 (w), 643 (vw), 533 (vw), 441 (m), 402 (w) cm^{-1}.

Preparation of [H(Et$_2$O)$_2$][Al(OC$_{10}$F$_{15}$)$_4$]

Li[Al(OC$_{10}$F$_{15}$)$_4$] (2.84 g, 1.65 mmol) containing impurities by alcohol C$_{10}$F$_{15}$OH and a solution of HCl in Et$_2$O (2 M, 40 mL, 80.0 mmol) were stirred for five days at r.t. The solvent was removed under reduced pressure. The target compound was extracted with o-DFB (3× 25 mL) and the solvent was removed afterwards under reduced pressure. The solid residue (2.31 g) was washed with CH$_2$Cl$_2$ (4× 10 mL), dried under reduced pressure and the colorless solid (1.99 g, 1.07 mmol, 65%) analyzed by NMR spectroscopy. Additionally, crystals suitable for scXRD could be obtained by storage of [H(Et$_2$O)$_2$][Al(OC$_{10}$F$_{15}$)$_4$] in o-DFB at -40 °C. ^{1}H NMR (300.18 MHz, 298 K, o-DFB): $\delta = 1.63$ (t, CH$_3$, 12H, [H(Et$_2$O)$_2$][Al(OC$_{10}$F$_{15}$)$_4$]), 4.27 (q, CH$_2$, 8H, [H(Et$_2$O)$_2$][Al(OC$_{10}$F$_{15}$)$_4$]), 16.20 (br. s, 1H, [H(Et$_2$O)$_2$][Al(OC$_{10}$F$_{15}$)$_4$]) ppm. ^{7}Li NMR (116.66 MHz, 298 K, o-DFB): $\delta = -0.1$ (br. s, 1Li, Li$^+$) ppm, only traces. ^{19}F NMR (282.45 MHz, 298 K, o-DFB): $\delta = -223.2$ (m, CF, 12F, [H(Et$_2$O)$_2$][Al(OC$_{10}$F$_{15}$)$_4$]), -121.3 (m, CF$_2$, 48F, [H(Et$_2$O)$_2$][Al(OC$_{10}$F$_{15}$)$_4$]) ppm. ^{27}Al NMR (78.22 MHz, 298 K, o-DFB): $\delta = 35.4$ (s, 1Al, [H(Et$_2$O)$_2$][Al(OC$_{10}$F$_{15}$)$_4$]) ppm. FTIR (Diamant, ATR): $\tilde{\nu} = 1392$ (vw), 1353 (vw), 1295 (vw), 1269 (vs), 1255 (m), 1192 (vw), 1108 (vw), 1016 (vw), 981 (m), 955 (vs), 905 (w), 760 (vw), 679 (vw), 652 (w), 533 (vw), 443 (w), 402 (w) cm^{-1}.

Preparation of Li[Al(OC$_{10}$F$_{15}$)$_4$]·(Et$_2$O)$_2$

[H(Et$_2$O)$_2$][Al(OC$_{10}$F$_{15}$)$_4$] (1.31 g, 0.759 mmol) and LiHMDS (0.127 g, 0.759 mmol, 1.0 eq.) were submitted into a Schlenk flask, suspended in o-DFB (7.0 mL) and stirred for 2.5 h at r.t. The solvent was removed under reduced pressure, the solid residue was washed with toluene (3× 5.0 mL) and dried under reduced pressure for several hours. The target compound was obtained as colorless solid (1.22 g, 0.681 mmol, 90%) and analyzed by NMR spectroscopy. ^{7}Li NMR (116.66 MHz, 298 K, THF): $\delta = -0.3$ (br. s, 1Li, Li$^+$) ppm. ^{19}F NMR (282.45 MHz, 298 K, THF): $\delta = -224.0$ (m, CF, 12F, Li[Al(OC$_{10}$F$_{15}$)$_4$]), -122.0 (m, CF$_2$, 48F, Li[Al(OC$_{10}$F$_{15}$)$_4$]) ppm. ^{27}Al NMR (78.22 MHz, 298 K, THF): $\delta = 34.6$ (s, 1Al, Li[Al(OC$_{10}$F$_{15}$)$_4$]) ppm.

Author contributions

A. Billion, M. Schorpp and I. Krossing conceptualized the study. A. Billion, R. Feser and L. Eisele performed syntheses and vibrational spectroscopic characterization. A. Billion and M. Schmitt performed quantum chemical calculations. M. Schorpp performed single crystal measurements. H. Scherer performed NMR spectroscopic analysis and data analysis. B. Butschke performed single crystal data analysis. T. Sonoda and H. Kawa provided the alcohol

HO-C$_{10}$F$_{15}$. A. Billion wrote the article. I. Krossing supervised the work and co-wrote the article.

Conflicts of interest

The authors declare no conflict of interest.

Acknowledgements

References

1 I. M. Riddlestone, A. Kraft, J. Schaefer and I. Krossing, *Angew. Chem., Int. Ed.*, 2018, **57**, 13982–14024.

2 T. A. Engesser, M. R. Lichtenthaler, M. Schleep and I. Krossing, *Chem. Soc. Rev.*, 2016, **45**, 789–899.

3 H. F. T. Klare, L. Albers, L. Süsse, S. Keess, T. Müller and M. Oestreich, *Chem. Rev.*, 2021, **121**, 5889–5985.

4 E. Y. Chen and T. J. Marks, *Chem. Rev.*, 2000, **100**, 1391–1434.

5 (*a*) S. P. Smidt, N. Zimmermann, M. Studer and A. Pfaltz, *Chem. – Eur. J.*, 2004, **10**, 4685–4693; (*b*) C. Margarita and P. G. Andersson, *J. Am. Chem. Soc.*, 2017, **139**, 1346–1356; (*c*) J. J. Verendel, O. Pàmies, M. Diéguez and P. G. Andersson, *Chem. Rev.*, 2014, **114**, 2130–2169.

6 (*a*) M. C. Lipke, A. L. Liberman-Martin and T. D. Tilley, *Angew. Chem., Int. Ed.*, 2017, **56**, 2260–2294; (*b*) A. Barthélemy, K. Glootz, H. Scherer, A. Hanske and I. Krossing, *Chem. Sci.*, 2022, **13**, 439–453.

7 A. B. A. Rupp and I. Krossing, *Acc. Chem. Res.*, 2015, **48**, 2537–2546.

8 A. Shyamsunder, W. Beichel, P. Klose, Q. Pang, H. Scherer, A. Hoffmann, G. K. Murphy, I. Krossing and L. F. Nazar, *Angew. Chem., Int. Ed.*, 2017, **56**, 6192–6197.

9 (*a*) K.-C. Lau, T. J. Seguin, E. V. Carino, N. T. Hahn, J. G. Connell, B. J. Ingram, K. A. Persson, K. R. Zavadil and C. Liao, *J. Electrochem. Soc.*, 2019, **166**, A1510–A1519; (*b*) P. Jankowski, Z. Li, Z. Zhao-Karger, T. Diemant, M. Fichtner, T. Vegge and J. M. G. Lastra, *Energy Storage Mater.*, 2022, **45**, 1133–1143.

10 (*a*) Z. Li, O. Fuhr, M. Fichtner and Z. Zhao-Karger, *Energy Environ. Sci.*, 2019, **12**, 3496–3501; (*b*) A. Shyamsunder, L. E. Blanc, A. Assoud and L. F. Nazar, *ACS Energy Lett.*, 2019, **4**, 2271–2276.

11 G. C. Fish, J. M. Moreno-Naranjo, A. Billion, D. Kratzert, E. Hack, I. Krossing, F. Nüesch and J.-E. Moser, *Phys. Chem. Chem. Phys.*, 2021, **23**, 23886–23895.

12 D. Gesevičius, A. Neels, S. Yakunin, E. Hack, M. V. Kovalenko, F. Nüesch and J. Heier, *ChemPhysChem*, 2018, **19**, 3356–3363.

13 A. G. Massey and A. J. Park, *J. Organomet. Chem.*, 1964, **2**, 245–250.

14 J. Foropoulos and D. D. DesMarteau, *Inorg. Chem.*, 1984, **23**, 3720–3723.

15 M. G. Fete, Z. Havlas and J. Michl, *J. Am. Chem. Soc.*, 2011, **133**, 4123–4131.

16 (*a*) I. Krossing and A. Reisinger, *Coord. Chem. Rev.*, 2006, **250**, 2721–2744; (*b*) I. Krossing, in *Comprehensive Inorganic Chemistry II*, Elsevier, 2013, pp. 681–705.

17 (*a*) S. Bulut, P. Klose and I. Krossing, *Dalton Trans.*, 2011, **40**, 8114–8124; (*b*) F. A. LeBlanc, A. Decken, T. S. Cameron, J. Passmore, J. M. Rautiainen and T. K. Whidden, *Inorg. Chem.*, 2017, **56**, 974–983.

18 I. Krossing, *Chem. – Eur. J.*, 2001, **7**, 490–502.

19 (*a*) S. M. Ivanova, B. G. Nolan, Y. Kobayashi, S. M. Miller, O. P. Anderson and S. H. Strauss, *Chem. – Eur. J.*, 2001, **7**, 503–510; (*b*) T. J. Barbarich, S. T. Handy, S. M. Miller, O. P. Anderson, P. A. Grieco and S. H. Strauss, *Organometallics*, 1996, **15**, 3776–3778; (*c*) T. J. Barbarich, S. M. Miller, O. P. Anderson and S. H. Strauss, *J. Mol. Catal. A: Chem.*, 1998, **128**, 289–331.

20 S. Tsujioka, B. G. Nolan, H. Takase, B. P. Fauber and S. H. Strauss, *J. Electrochem. Soc.*, 2004, **151**, A1418.

21 U. P. Preiss, G. Steinfeld, H. Scherer, A. M. T. Erle, B. Benkmil, A. Kraft and I. Krossing, *Z. Anorg. Allg. Chem.*, 2013, **639**, 714–721.

22 J. J. Rockwell, G. M. Kloster, W. J. DuBay, P. A. Grieco, D. F. Shriver and S. H. Strauss, *Inorg. Chim. Acta*, 1997, **263**, 195–200.

23 I. M. Riddlestone, S. Keller, F. Kirschenmann, M. Schorpp and I. Krossing, *Eur. J. Inorg. Chem.*, 2019, **2019**, 59–67.

24 Y. Sun, M. V. Metz, C. L. Stern and T. J. Marks, *Organometallics*, 2000, **19**, 1625–1627.

25 (*a*) J. B. Lambert and Y. Zhao, *Angew. Chem., Int. Ed. Engl.*, 1997, **36**, 400–401; (*b*) A. Schäfer, M. Reissmann, A. Schäfer, W. Saak, D. Haase and T. Müller, *Angew. Chem., Int. Ed.*, 2011, **50**, 12636–12638.

26 T. Köchner, T. A. Engesser, H. Scherer, D. A. Plattner, A. Steffani and I. Krossing, *Angew. Chem., Int. Ed.*, 2012, **51**, 6529–6531.

27 (*a*) T. A. Engesser, C. Friedmann, A. Martens, D. Kratzert, P. J. Malinowski and I. Krossing, *Chem. – Eur. J.*, 2016, **22**, 15085–15094; (*b*) T. W. Hayton, P. Legzdins and W. B. Sharp, *Chem. Rev.*, 2002, **102**, 935–992.

28 M. Kuprat, M. Lehmann, A. Schulz and A. Villinger, *Organometallics*, 2010, **29**, 1421–1427.

29 S. B. Beil, S. Möhle, P. Enders and S. R. Waldvogel, *Chem. Commun.*, 2018, **54**, 6128–6131.

30 M. Niemann, B. Neumann, H.-G. Stammler and B. Hoge, *Angew. Chem., Int. Ed.*, 2019, **58**, 8938–8942.

31 A. Wiesner, T. W. Gries, S. Steinhauer, H. Beckers and S. Riedel, *Angew. Chem.*, 2017, **129**, 8375–8378.

32 A. Reisinger, N. Trapp, I. Krossing, S. Altmannshofer, V. Herz, M. Presnitz and W. Scherer, *Angew. Chem., Int. Ed.*, 2007, **46**, 8295–8298.

33 (*a*) J. K. Kochi, *Acc. Chem. Res.*, 1992, **25**, 39–47; (*b*) M. Schorpp, T. Heizmann, M. Schmucker, S. Rein, S. Weber and I. Krossing, *Angew. Chem., Int. Ed.*, 2020, **59**, 9453–9459 https://onlinelibrary.wiley.com/doi/10.1002/anie.202002768(*c*) M. Sellin, C. Friedmann, M. Mayländer, S. Richert and I. Krossing, *Chem. Sci.*, 2022, **13**, 9147–9158.

34 C. Armbruster, J. Hunger and I. Krossing, Unpublished data, 26.11.22.

35 M. Rohde, L. O. Müller, D. Himmel, H. Scherer and I. Krossing, *Chem. – Eur. J.*, 2014, **20**, 1218–1222.

36 D. Kratzert, J. J. Holstein and I. Krossing, *J. Appl. Crystallogr.*, 2015, **48**, 933–938.

37 D. Kratzert and I. Krossing, *J. Appl. Crystallogr.*, 2018, **51**, 928–934.

38 I. Krossing and I. Raabe, *Chem. – Eur. J.*, 2004, **10**, 5017–5030.

39 S. Grimme, J. Antony, S. Ehrlich and H. Krieg, *J. Chem. Phys.*, 2010, **132**, 154104.

40 S. Grimme, S. Ehrlich and L. Goerigk, *J. Comput. Chem.*, 2011, **32**, 1456–1465.

41 P. Erdmann, J. Leitner, J. Schwarz and L. Greb, *ChemPhysChem*, 2020, **21**, 987–994.

42 R. Herrero, J. Z. Dávalos, J.-L. M. Abboud, I. Alkorta and M. Mishima, *Int. J. Mass Spectrom.*, 2007, **267**, 302–307 https://www.researchgate.net/publication/216043302_The_intrinsic_gas-phase_acidities_of_bridgehead_alcohols_An_experimental_FT-ICR_and_computational_study.

43 (*a*) M. Zhang, M. M. R. Badal, M. Pasikowska, T. Sonoda, M. Mishima, H. Fukaya, T. Ono, H.-U. Siehl, J.-L. M. Abboud and I. A. Koppel, *Bull. Chem. Soc. Jpn.*, 2014, **87**, 825–834; (*b*) J.-L. M. José-Luis, M. Abboud, M. Mishima and T. Sonoda, *Proc. Est. Acad. Sci., Chem.*, 2005, **54**, 60.

44 N. Trapp, H. Scherer, S. A. Hayes, R. J. F. Berger, A. Kütt, N. W. Mitzel, J. Saame and I. Krossing, *Phys. Chem. Chem. Phys.*, 2011, **13**, 6184–6191.

45 A. Kütt, I. Leito, I. Kaljurand, L. Soovӓli, V. M. Vlasov, L. M. Yagupolskii and I. A. Koppel, *J. Org. Chem.*, 2006, **71**, 2829–2838.

46 R. W. Taft, I. A. Koppel, R. D. Topsom and F. Anvia, *J. Am. Chem. Soc.*, 1990, **112**, 2047–2052.

47 (*a*) K. O. Christe, D. A. Dixon, D. McLemore, W. W. Wilson, J. A. Sheehy and J. A. Boatz, *J. Fluorine Chem.*, 2000, **101**, 151–153; (*b*) T. E. Mallouk, G. L. Rosenthal, G. Mueller, R. Brusasco and N. Bartlett, *Inorg. Chem.*, 1984, **23**, 3167–3173.

48 H. Böhrer, N. Trapp, D. Himmel, M. Schleep and I. Krossing, *Dalton Trans.*, 2015, **44**, 7489–7499.

49 P. Erdmann and L. Greb, *ChemPhysChem*, 2021, **22**, 935–943.

50 L. O. Müller, D. Himmel, J. Stauffer, G. Steinfeld, J. Slattery, G. Santiso-Quiñones, V. Brecht and I. Krossing, *Angew. Chem., Int. Ed.*, 2008, **47**, 7659–7663.

51 A. Wiesner, L. Fischer, S. Steinhauer, H. Beckers and S. Riedel, *Chem. – Eur. J.*, 2019, **25**, 10441–10449.

52 *CRC Handbook of chemistry and physics*, ed. W. M. Haynes, ed., CRC Press, Boca Raton, London, New York, 97th edn, 2017.

53 P. Dabringhaus, A. Barthélemy and I. Krossing, *Z. Anorg. Allg. Chem.*, 2021, **647**, 1660–1673.

54 I. Krossing, H. Brands, R. Feuerhake and S. Koenig, *J. Fluorine Chem.*, 2001, **112**, 83–90.

55 A. Decken, H. D. B. Jenkins, G. B. Nikiforov and J. Passmore, *Dalton Trans.*, 2004, 2496–2504.

56 A. Martens, P. Weis, M. C. Krummer, M. Kreuzer, A. Meierhöfer, S. C. Meier, J. Bohnenberger, H. Scherer, I. Riddlestone and I. Krossing, *Chem. Sci.*, 2018, **9**, 7058–7068.

57 J. Frötschel-Rittmeyer, M. Holthausen, C. Friedmann, D. Röhner, I. Krossing and J. J. Weigand, *Sci. Adv.*, 2022, **8**, eabq8613.

58 M. Gonsior, I. Krossing and N. Mitzel, *Z. Anorg. Allg. Chem.*, 2002, **628**, 1821.

59 I. Krossing and A. Reisinger, *Eur. J. Inorg. Chem.*, 2005, **2005**, 1979–1989.

60 A. Schmidt, H. Koger, A. Barthélemy, G. Studer, B. Esser and I. Krossing, *Batteries Supercaps*, 2022, **5**(12), e202200340, DOI: 10.1002/batt.202200340.

61 A. Reisinger, N. Trapp and I. Krossing, *Organometallics*, 2007, **26**, 2096–2105.

62 L. Brammer, E. A. Bruton and P. Sherwood, *Cryst. Growth Des.*, 2001, **1**, 277–290.

63 P. R. Spackman, M. J. Turner, J. J. McKinnon, S. K. Wolff, D. J. Grimwood, D. Jayatilaka and M. A. Spackman, *J. Appl. Crystallogr.*, 2021, **54**, 1006–1011.

64 J. Cosier and A. M. Glazer, *J. Appl. Crystallogr.*, 1986, **19**, 105–107.

65 *SAINT V8.38A*, Bruker AXS, Madison, Wisconsin, USA, 2015.

66 L. Krause, R. Herbst-Irmer, G. M. Sheldrick and D. Stalke, *J. Appl. Crystallogr.*, 2015, **48**, 3–10.

67 G. M. Sheldrick, *Acta Crystallogr., Sect. A: Found. Crystallogr.*, 2015, **71**, 3–8.

68 G. M. Sheldrick, *Acta Crystallogr., Sect. C: Cryst. Struct. Commun.*, 2015, **71**, 3–8.

69 C. B. Hübschle, G. M. Sheldrick and B. Dittrich, *J. Appl. Crystallogr.*, 2011, **44**, 1281–1284.

70 D. Kratzert, *FinalCif, V104*. Available at: https://dkratzert.de/finalcif.html.

71 O. V. Dolomanov, L. J. Bourhis, R. J. Gildea, J. A. K. Howard and H. Puschmann, *J. Appl. Crystallogr.*, 2009, **42**, 339–341.

72 (*a*) M. von Arnim and R. Ahlrichs, *J. Comput. Chem.*, 1998, **19**, 1746–1757; (*b*) O. Treutler and R. Ahlrichs, *J. Chem. Phys.*, 1995, **102**, 346–354.

73 (*a*) J. P. Perdew, *Phys. Rev. B: Condens. Matter*, 1986, **33**, 8822–8824; (*b*) J. P. Perdew, *Phys. Rev. B: Condens. Matter*, 1986, **34**, 7406.

74 S. Grimme, J. G. Brandenburg, C. Bannwarth and A. Hansen, *J. Chem. Phys.*, 2015, **143**, 54107.

75 (*a*) M. Sierka, A. Hogekamp and R. Ahlrichs, *J. Chem. Phys.*, 2003, **118**, 9136–9148; (*b*) F. Weigend, *Phys. Chem. Chem. Phys.*, 2006, **8**, 1057–1065; (*c*) R. Ahlrichs, *Phys. Chem. Chem. Phys.*, 2004, **6**, 5119.

76 A. Schäfer, H. Horn and R. Ahlrichs, *J. Chem. Phys.*, 1992, **97**, 2571–2577.

77 F. Weigend, M. Häser, H. Patzelt and R. Ahlrichs, *Chem. Phys. Lett.*, 1998, **294**, 143–152.

78 P. Deglmann, F. Furche and R. Ahlrichs, *Chem. Phys. Lett.*, 2002, **362**, 511–518.

79 A. Klamt and G. Schüürmann, *J. Chem. Soc., Perkin Trans. 2,*, 1993, 799–805.

80 (*a*) C. Riplinger, B. Sandhoefer, A. Hansen and F. Neese, *J. Chem. Phys.*, 2013, **139**, 134101; (*b*) D. G. Liakos, M. Sparta, M. K. Kesharwani, J. M. L. Martin and F. Neese, *J. Chem. Theory Comput.*, 2015, **11**, 1525–1539.

81 (*a*) T. H. Dunning, *J. Chem. Phys.*, 1989, **90**, 1007–1023; (*b*) R. A. Kendall, T. H. Dunning and R. J. Harrison, *J. Chem. Phys.*, 1992, **96**, 6796–6806; (*c*) F. Weigend, A. Köhn and C. Hättig, *J. Chem. Phys.*, 2002, **116**, 3175–3183; (*d*) N. B. Balabanov and K. A. Peterson, *J. Chem. Phys.*, 2005, **123**, 64107; (*e*) D. H. Bross, J. G. Hill, H.-J. Werner and K. A. Peterson, *J. Chem. Phys.*, 2013, **139**, 94302.

82 S. Kozuch and J. M. L. Martin, *Phys. Chem. Chem. Phys.*, 2011, **13**, 20104–20107.

83 F. Weigend and R. Ahlrichs, *Phys. Chem. Chem. Phys.*, 2005, **7**, 3297–3305.